

AN APPARATUS TO MEASURE DROPWISE CONDENSATION
HEAT TRANSFER COEFFICIENTS OF STEAM

Larry Ralph Sharp

DUDLEY KNOX LIBRARY
NAVAL POSTGRADUATE SCH
MONTEREY CA 93940

NAVAL POSTGRADUATE SCHOOL

Monterey, California



THESIS

AN APPARATUS TO MEASURE DROPWISE CONDENSATION
HEAT TRANSFER COEFFICIENTS OF STEAM

by

Larry Ralph Sharp

March 1978

Thesis Advisor:

P. J. Marto

T183191

Unclassified

SECURITY CLASSIFICATION OF THIS PAGE (When Date Entered)

REPORT DOCUMENTATION PAGE		READ INSTRUCTIONS BEFORE COMPLETING FORM
1. REPORT NUMBER	2. GOVT ACCESSION NO.	3. RECIPIENT'S CATALOG NUMBER
4. TITLE (and Subtitle) An Apparatus to Measure Dropwise Condensation Heat Transfer Coeffi- cients of Steam		5. TYPE OF REPORT & PERIOD COVERED Master's Thesis; March 1978
7. AUTHOR(s) Larry Ralph Sharp		6. PERFORMING ORG. REPORT NUMBER
9. PERFORMING ORGANIZATION NAME AND ADDRESS Naval Postgraduate School Monterey, California 93940		8. CONTRACT OR GRANT NUMBER(s)
11. CONTROLLING OFFICE NAME AND ADDRESS Naval Postgraduate School Monterey, California 93940		10. PROGRAM ELEMENT, PROJECT, TASK AREA & WORK UNIT NUMBERS
14. MONITORING AGENCY NAME & ADDRESS (if different from Controlling Office) Naval Postgraduate School Monterey, California 93940		12. REPORT DATE March 1978
		13. NUMBER OF PAGES
		15. SECURITY CLASS. (of this report) Unclassified
		15a. DECLASSIFICATION/DOWNGRADING SCHEDULE
16. DISTRIBUTION STATEMENT (of this Report) Approved for public release; distribution unlimited.		
17. DISTRIBUTION STATEMENT (of the abstract entered in Block 20, if different from Report)		
18. SUPPLEMENTARY NOTES		
19. KEY WORDS (Continue on reverse side if necessary and identify by block number) Dropwise Condensation, Thin Film Resistance Thermometer, Thickness Dependence.		
20. ABSTRACT (Continue on reverse side if necessary and identify by block number) An experimental apparatus was designed and constructed for the purpose of determining dropwise condensation heat transfer coefficients on condensing surfaces of different thickness. The equipment included a completely self con- tained condensing chamber which enclosed both the boiler and condensing surface. Variable temperature cooling water		

was utilized to control the heat flux.

A thin film resistance thermometer was constructed to obtain the average surface temperature of the condensing surface. Inability to obtain linear and repeatable calibration data with this thermometer resulted in its being discarded. An intrinsic thermocouple was used in lieu of of the thin film resistance thermometer.

Experimental data was taken for a 0.51 mm thick stainless steel condensing surface. Results indicated the existence of a condensing curve similar in shape to the characteristic boiling curve represented by heat flux versus $T_{\text{vap}} - T_{\text{wall}}$.

APPROVED FOR PUBLIC RELEASE; DISTRIBUTION UNLIMITED

An Apparatus to Measure Dropwise Condensation
Heat Transfer Coefficients of Steam

by

Larry Ralph Sharp
Lieutenant, United States Navy
B.S., University of Utah, 1970

Submitted in partial fulfillment of the
requirements for the degree of

MASTER OF SCIENCE IN MECHANICAL ENGINEERING

from the

NAVAL POSTGRADUATE SCHOOL
March 1978

سندھ
54354
ت. 1

ABSTRACT

An experimental apparatus was designed and constructed for the purpose of determining dropwise condensation heat transfer coefficients on condensing surfaces of different thickness. The equipment included a completely self contained condensing chamber which enclosed both the boiler and condensing surface. Variable temperature cooling water was utilized to control the heat flux.

A thin film resistance thermometer was constructed to obtain the average surface temperature of the condensing surface. Inability to obtain linear and repeatable calibration data with this thermometer resulted in its being discarded. An intrinsic thermocouple was used in lieu of the thin film resistance thermometer.

Experimental data was taken for a 0.51 mm thick stainless steel condensing surface. Results indicated the existence of a condensing curve similar in shape to the characteristic boiling curve represented by heat flux versus $T_{\text{vap}} - T_{\text{wall}}$.

TABLE OF CONTENTS

I.	INTRODUCTION-----	12
A.	THE DROPWISE CONDENSATION PROCESS-----	12
B.	EFFECT OF CONDENSING SURFACE THICKNESS ON DROPWISE CONDENSATION HEAT TRANSFER-----	14
C.	OBJECTIVES OF THIS WORK-----	18
II.	DESCRIPTION OF EXPERIMENTAL APPARATUS-----	19
A.	CONDENSING CHAMBER-----	19
1.	Condenser Test Section-----	20
a.	Front Chamber-----	20
b.	Rear Chamber-----	21
c.	Cooling Water Inlet Tube-----	21
d.	Cooling Water Outlet Tube-----	21
e.	Test Surfaces-----	22
2.	Immersion Heaters-----	23
3.	Auxiliary Condenser-----	23
4.	End Plates-----	24
5.	Observation Port-----	24
B.	SUPPORT SYSTEMS-----	25
1.	Cooling Water System-----	25
2.	Vacuum System-----	26
3.	Refrigeration System-----	28
C.	INSTRUMENTATION-----	28
1.	Temperature Measurement System-----	29
a.	Thermocouples-----	29
b.	Thin Film Resistance Thermometers-----	30
c.	Intrinsic Thermocouple-----	32

2. Flowmeter-----	33
3. Mercury Manometer-----	33
III. EXPERIMENTAL PROCEDURES-----	35
A. TEST SURFACE PREPARATION-----	35
B. START-UP AND OPERATION-----	35
C. HEAT TRANSFER DATA REDUCTION-----	37
1. Heat Flux Determination-----	37
2. Temperature Determination-----	38
3. Heat Transfer Coefficient Determination-----	39
IV. PRESENTATION AND DISCUSSION OF RESULTS-----	40
A. GENERAL-----	40
B. DROPWISE CONDENSATION RESULTS-----	40
C. THIN FILM RESISTANCE THERMOMETER-----	42
V. CONCLUSIONS AND RECOMMENDATIONS-----	44
A. CONCLUSIONS-----	44
B. RECOMMENDATIONS FOR FURTHER WORK-----	44
APPENDIX A: PHOTOGRAPHIC ETCHING PROCEDURES-----	45
APPENDIX B: CALIBRATION OF INSTRUMENTS-----	47
1. Thermocouples-----	47
2. Thin Film Resistance Thermometer-----	48
3. Intrinsic Thermocouple-----	49
4. Flowmeter-----	49
APPENDIX C: UNCERTAINTY ANALYSIS-----	51
LIST OF REFERENCES-----	90
INITIAL DISTRIBUTION LIST-----	92

LIST OF TABLES

Table

I	FLOWMETER CALIBRATION SUMMARY-----	56
II	DATA CALCULATIONS WITH UNCERTAINTY LIMITS-----	57

LIST OF FIGURES

<u>Figure</u>	<u>Title</u>	
1	Schematic Drawing of Experimental Apparatus-----	58
2	Photographic Front View of Experimental Apparatus-----	59
3	Photographic Rear View of Experimental Apparatus-----	60
4	Details of Pyrex Glass Cross-----	61
5	Photograph of the Front, Right Side of the Condensing Chamber-----	62
6	Photograph of the Front of the Condensing Chamber-----	63
7	Photograph of the Front, Left Side of the Condensing Chamber-----	64
8	Photograph of Rear of the Condensing Chamber-----	65
9	Photograph of Rear, Left Side of the Condensing Chamber-----	66
10	Details of Condenser Test Section-----	67
11	Photograph of Condenser Test Section-----	68
12	Details of Test Section Front Chamber-----	69
13	Photograph of Test Section Front Chamber-----	70
14	Details of Test Section Rear Chamber-----	71
15	Details of Cooling Water Inlet and Outlet Tubes-----	72
16	Side View of Test Section Rear Chamber With Inlet and Outlet Tubes Installed-----	73
17	Rear View of Test Section Rear Chamber With Inlet and Outlet Tubes Installed-----	74
18	Details of Test Surface-----	75
19	Photograph of "O"-ring Seal on Front Chamber Face-----	76

20	Photograph of "O"-ring Seal on Back of Front Chamber-----	77
21	Details of Test Surface Retaining Ring-----	78
22	Photograph of Retaining Ring and Test Surface on Front Chamber Face-----	79
23	Details of Bottom End Plate-----	80
24	Details of Top End Plate-----	81
25	Details of Observation Port Support Frame-----	82
26	Photograph of Storage Reservoir-----	83
27	Details of Moisture Separator-----	84
28	Photograph of Refrigeration System-----	85
29	Photograph of Test Surface Showing Etched Titanium Meander Thermometer-----	86
30	Details of Test Surface Installation In Condenser Test Section-----	87
31	Temperature Fluctuation on the Condensing Surface Recorded by the Intrinsic Thermo- couple at a ΔT of 6.97°C-----	88
32	Comparison of Experimental Data with the Condensing Curve Proposed by Takeyama[8]-----	89

NOMENCLATURE

A	Area [mm ²]
C _{pcw}	Cooling-water specific heat [kJ/kg - °C]
d	Diameter [mm]
g	Acceleration of gravity [m/sec ²]
g _c	Gravitational constant [kg-m/N-sec ²]
\bar{h}_{ss}	Average steam side heat transfer coefficient [kW/m ² - °C]
k	Thermal conductivity [W/m - °C]
\dot{m}_{cw}	Cooling water mass flow rate [kg/sec]
m	Mass [kg]
P	Pressure [mm H _g]
q	Heat transfer rate [W]
q/A	Heat flux [W/m ²]
t	Time [sec]
T _{cwin}	Cooling water inlet temperature [°C]
T _{cwout}	Cooling water outlet temperature [°C]
T _{vap}	Saturated steam temperature [°C]
T _{wall}	Condensing surface temperature [°C]
T _{sat}	Saturated steam temperature [°C]
ΔT _{cw}	Cooling water temperature difference [°C]

ACKNOWLEDGMENTS

The author wishes to thank Mr. Ken Graham, the Naval Postgraduate School Chemist, who prepared several different chemical etchants and promoters for use in this work.

Special thanks go to Mr. George Bixler and Mr. Thomas Christian for their expert help in constructing and instrumenting the experimental apparatus.

Sincere thanks go to Professor Paul Marto whose patience and knowledge provided the necessary guidance to bring this work to completion.

Lastly, but not least, the author wishes to express his thanks and appreciation to his wife, Ann, whose understanding and unfailing support made this work possible.

I. INTRODUCTION

One of the goals of propulsion steam plant designers in recent years has been to reduce the size and weight of steam propulsion plants while maintaining or even increasing plant output. With more emphasis placed on lighter, faster ships and energy conservation in the last few years, this goal has become even more necessary.

One component of a steam plant where considerable savings could be made is the main condenser. A large amount of research is currently being performed into the various ways to enhance the heat transfer in two phase heat exchangers. One of the areas of enhancement, seriously being studied is that of dropwise condensation. It has been discovered that dropwise condensation heat transfer coefficients can be as much as ten times greater than that of filmwise condensation coefficients.

A. THE DROPWISE CONDENSATION PROCESS

Since the discovery of dropwise condensation by Schmidt, Schuring, and Sellschopp [1] in 1930, two basic theories have been proposed to explain this condensation phenomenon.

Jakob [2] suggested that a thin film of water coated the condensing surface which constantly drew thicker and eventually separated into droplets. The droplets then coalesced and rolled off the surface, sweeping it of other

drops. It was this dry surface in direct contact with the saturated vapor, Jakob said, that explained the high heat transfer rates.

A second theory was proposed in 1935 by Tammann and Boehme [3] who observed that droplets forming on the condensing surface seemed to form a pattern that did not vary as continuous condensation occurred. This seemed to suggest the existence of specific nucleation sites rather than a thin film layer.

The nucleation theory has been generally accepted as the explanation for drop growth. For example, using both optical examinations and thermodynamic considerations, Umur and Griffith [4] concluded that the majority of the energy being transferred from the saturated vapor to the cooling surface passed through the drops with no net condensation taking place in the area between the drops.

The dropwise condensation process can be divided into four basic phases as described by Graham and Aerni [5]:

1. Nucleation

When the saturated vapor comes in contact with the cooled condensing surface, small drops (0.5 micron diameter) begin to form at discrete nucleation sites. If the surface is hydrophobic (non-wetting), droplets will be formed versus a thin film layer.

2. Condensation and Coalescence

As condensation continues, each of the small drops grows very quickly. Since there are numerous small drops on the surface, they eventually coalesce and form into one

drop. The drops continue this process until they can just be seen by the naked eye (approximately 0.1 mm diameter).

3. Coalescence

When a drop reaches approximately 0.15 mm diameter, the conduction resistance through the drop becomes so great that condensation no longer occurs on the drop surface. At this point the drop can grow only by coalescing with smaller nearby drops.

4. Departure

At the point where the drop reaches 2 to 3 mm in diameter, the gravitational forces overcome the surface tension forces and the drop begins to slide down the surface sweeping out a path as it goes. This sweeping action by the drop tends to remove the larger "inactive" drops making room for new, small drops to grow, which actually enhances the heat transfer.

This completes the cycle which in actuality lasts on the order of milliseconds.

B. EFFECT OF CONDENSING SURFACE THICKNESS ON DROPWISE CONDENSATION HEAT TRANSFER

Extensive experimental and analytical research has been conducted in the area of dropwise condensation concerning pressure, surface thermal conductivity, surface inclination, type of promoter, drop size, surface finish, etc. One area that still remains relatively untouched is the effect of condensing surface thickness on the heat transfer rate in dropwise condensation.

In condenser design today, considerable thought has been given to the use of titanium as a tube material versus copper-nickel. Because of the higher strength and lower specific weight of titanium, a 55 percent reduction in tube wall thickness could be obtained with approximately the same heat transfer rate. This reduction in wall thickness from 1.25 mm for copper-nickel to 0.56 mm for titanium would also account for a considerable reduction in total condenser weight.

With the small amount of data available concerning surface thickness effects on heat transfer it is quite reasonable to question the plausibility of decreased tube wall thickness in dropwise condensation. In a paper by Magrini and Nannei [6] concerning heating wall thickness effects in nucleate pool boiling, it was shown that heat transfer coefficients can very definitely be affected by the wall thickness of the heating surface. In fact it was recently concluded by Chuck and Myers [7] that for small temperature differences, low thermal conductivity materials exhibit an increase in heat transfer coefficient with decreasing wall thickness. Since nucleate pool boiling involves a physical mechanism which is similar to dropwise condensation, it is reasonable to believe there must exist a similar condenser wall thickness relationship for dropwise condensation.

Takeyama and Shimizu [8] proposed the existence of a condensing curve similar to the boiling curve shown by heat flux versus temperature difference. The existence of such a

curve again strongly suggests a physical relation between the two mechanisms of nucleate pool boiling and dropwise condensation.

Considerable research has been conducted into the effect of surface thermal conductivity on heat transfer coefficients in the dropwise condensation mode. For low conductivity materials, Mikic [9] deduced from available experimental data that an additional significant resistance to heat flow existed due to the nonuniform condensing surface temperature distribution. This resistance, which he referred to as a constriction resistance caused by the constriction of heat flow lines in a plate near the condensing surface, led to the fin analogy referred to by Hurst and Olson [10]. In their paper, they concluded that during dropwise condensation the condensing surface is analogous to an extended surface in a convective-cooling application, transferring heat from the drops laterally through the surface and into the cooling fluid. They also implied that this fin analogy suggested the existence of a minimum condensing wall thickness below which the wall fails to function well as a fin. Hannemann and Mikic [11, 12] presented an analysis and an experimental investigation to show that a finite thermal resistance caused by the nonuniform surface heat flux does in fact exist and is dependent on the thermal properties of the condensing surface. In their analysis the constriction resistance associated with a single conducting droplet and its surrounding active condensation area was modeled as a

cylindrical element of condensing surface of finite thickness. Using a finite element solution to solve the problem they found that a surface thickness to cylinder radius ratio of four produced the maximum constriction effect. A correlation relating constriction resistance to surface thermal properties was also developed. This correlation was found to compare quite well with existing data.

In a recent paper, Hannemann [13] analysed the effect of condensing surface thickness on constriction resistance in dropwise condensation using a model similar to that of Ref. 11. Using an analytical expression for the temperature distribution in the model, Hannemann was able to modify the earlier correlation of Ref. 10 to include the effect of wall thickness on constriction resistance.

As is evident from reviewing the preceding papers, little, if any, direct correlation has been established between condensing wall thickness and heat transfer coefficient for dropwise condensation. Similarly, very little intentional experimental research has been conducted regarding this question.

Morgan [14] in his investigation of different factors affecting dropwise condensation unintentionally discovered a strange phenomenon. He found that for a copper surface the heat transfer coefficient increased by a factor of five when the condensing surface thickness was increased from 0.051 mm to 3.18 mm. These findings again suggest a relationship between condensing wall thickness and heat transfer coefficient for dropwise condensation.

C. OBJECTIVES OF THIS WORK

The analytical conclusions of various researchers cited and the experimental results of Morgan [14] concerning condensing wall thickness and heat transfer coefficient show very plainly the need for experimental research in this area.

Therefore the objectives of this study are:

1. To design and construct an experimental apparatus capable of condensing saturated steam on condensing surfaces of various thicknesses while varying the temperature of the cooling fluid.
2. To examine the Takeyama and Shimizu [8] condensing curve and to experimentally reproduce such a curve for a stainless steel condensing surface using the newly constructed experimental apparatus.
3. To obtain precise experimental data to develop a series of dropwise condensation curves for varying thicknesses of condensing surface.

II. DESCRIPTION OF EXPERIMENTAL APPARATUS

One of the objectives of this work was to study the effect of condensing surface thickness on the heat transfer coefficient for dropwise condensation. Figure 1 is a system schematic showing the layout of the apparatus used in attempting to accomplish this objective. Figures 2 and 3 illustrate the exact layout of the experimental apparatus.

The experimental apparatus can be divided into three major components: 1) the condensing chamber, 2) the support systems and 3) the instrumentation.

A. CONDENSING CHAMBER

The condensing chamber was constructed using a thick walled Pyrex glass cross 457.2 mm by 304.8 mm (See Figure 4). Each of the legs of the cross contained an "O" ring groove for vacuum sealing. The primary goal behind designing a new apparatus for this experiment was to build a self-contained chamber where boiling and condensing could take place in the same closed container. The Pyrex glass cross met this criterion so all plans were developed using this chamber as a building block for the other components.

The bottom of the cross was used for the immersion heaters while the upper portion was configured for an auxiliary condenser. Of the two smaller side legs, one was ideal for the test section while the opposite leg made an excellent observation port. All connections for the vacuum system, manometer, thermocouples and auxiliary

condenser were made through the top plate. Figures 5 through 9 illustrate the details of the condensing chamber.

1. Condenser Test Section

The condenser test section (See Figures 10 and 11) consisted of five main parts: 1) the front chamber, 2) the rear chamber, 3) the cooling water inlet tube, 4) the cooling water outlet tube and 5) the test surfaces. These five components are illustrated in Figures 12 through 18. Type 6 white nylon was used to construct the test section because of its relatively low thermal conductivity ($k = .173 \frac{\text{Watts}}{\text{m}^{\circ}\text{C}}$) and freedom from outgassing when hot. The vacuum seal between the condenser test section and the Pyrex glass cross was provided by the use of an "O" ring.

a. Front Chamber

The front chamber was designed to provide maximum contact between test surface and condensing steam by making the test surface flush with the inside cylindrical face of the Pyrex glass cross. In the front face of the chamber, a 41.27 mm diameter by 3.17 mm deep cylindrical pocket was machined so the test surface could be inserted. The test surface was sealed to the chamber face by machining an "O" ring groove into the nylon and using an "O" ring of the appropriate size (See Figure 19). The test surface was held in place against the "O" ring seal by a circular retaining ring. Figure 20 shows the "O" ring seal on the back face of the front chamber. A 38.1 mm diameter by 3.17 mm deep groove was machined for this "O" ring which

provided a water tight seal between the front and rear chambers.

b. Rear Chamber

Figure 14 shows in detail the design of the rear chamber. Holes drilled in the milled section and the back of the chamber provide attachment points for the cooling water inlet and outlet tubes.

c. Cooling Water Inlet Tube

Cooling water was directed onto the back side of the test surface by the cooling water inlet tube. Considerable thought was given to the design of the cooling water inlet. In an attempt to provide a smooth flow of water across the test surface, the inlet tube was designed such that a constant flow area existed from the inlet to the outlet of the test section.

Watertight sealing of the inlet tube was accomplished by machining an "O" ring groove into the neck of the tube. An "O" ring was then inserted into the groove and a retaining ring bolted to the rear chamber to secure the inlet tube in place (See Figure 17.).

d. Cooling Water Outlet Tube

The inside diameter of the cooling water outlet tube was purposely made small to provide a back pressure to the flow through the test section.

Similar to the inlet tube the outlet tube was sealed with an "O" ring and a retaining ring bolted to the rear chamber (See Figure 17.).

e. Test Surfaces

Six test surfaces of 0.127, 0.241, 0.508, 0.10, 2.09 and 3.05 mm thickness were made as samples for this experimental work.

The first three thicknesses were produced by cutting 41.28 mm diameter discs from 304 stainless steel shim stock. Stainless steel backing rings with the same outside diameter as the discs and an inside diameter of 28.58 mm were then machined to various thicknesses. The machining of the backing ring was performed such that the disc and backing ring together gave a total thickness of 3.18 mm. This insured that all of the test surfaces would fit into the test section in a uniform manner. The stainless steel discs and backing rings were brazed together by Pyromet Industries of San Carlos, California. Using a compound consisting of 35 percent gold and 65 percent copper, the two pieces were brazed in a high temperature dry nitrogen oven. This process provided an air tight seal between the backing rings and discs while preventing any warpage of the thin material.

The remaining three test surfaces were machined from 304 stainless steel bar stock. Because of the thicker material, discs and backing rings could be machined in one piece preventing any need for brazing. At this point the thin film resistance thermometers were installed on the test surfaces, as explained in section II-C-1b and Appendix A.

The completed test surfaces were secured to the condenser test section by a 57.5 mm diameter nylon

retaining ring held in place by eight stainless steel screws. The inside surface of the ring was chamfered at a 35 degree angle to allow the condensate to drain away from the test surface. A 3.0 mm by 6.5 mm groove was milled in the underside of each wall of the retaining ring to provide clearance for the copper wire connection posts. Figure 21 illustrates the details of the test surface retaining ring. Figure 22 is a photograph of the condenser test section, showing the test surface and retaining ring.

2. Immersion Heaters

The boiler section of the condensing chamber consisted of five 250 watt immersion heaters obtained from Watlow Electric Company. The heating elements, 6.35 mm in diameter and 44.45 mm long, were seal brazed to 1/4 inch standard pipe fittings. The heaters were then mounted in the bottom end plate in the pattern illustrated in Figure 23. The electrical leads were connected in parallel to a Powerstat variable transformer to give the capability of varying the power input to the heaters.

3. Auxiliary Condenser

Although the majority of the steam was designed to condense on the test surface, an auxiliary condenser was designed and installed in the upper portion of the condensing chamber. This allowed for better control of the steam pressure and provided for some flow of steam past the test surface. A bypass valve was installed to control the cooling water flow rate through the auxiliary condenser.

The auxiliary condenser consisted of approximately three meters of 6.35 mm O.D. thin wall copper tubing formed into a dual pass cylindrical condenser measuring 127.0 mm deep by 63.5 mm in diameter.

4. End Plates

Two 266.7 mm diameter, 9.53 mm thick end plates were manufactured from 304 stainless steel bar stock. Stainless steel was chosen because of its anti-corrosion characteristics and strength.

Figure 23 illustrates the details of the bottom end plate and the immersion heater layout.

Figure 24 shows the top end plate and location of the different fittings. Swagelok pressure fittings were used to provide a vacuum tight seal for the various auxiliary condenser, vacuum, manometer and thermocouple connections in the top end plate.

The top and bottom end plates were each held in place by eight 6.5 mm long bolts secured to tapered flanges. The flanges were made in two pieces and fit onto the taper of the Pyrex glass cross. Thin gasket material was used to avoid direct contact between the metal flanges and the glass. Vacuum tight seals were maintained by "O" rings between the end plates and the glass cross.

5. Observation Port

The observation port consisted of two Pyrex brand glass discs 95.25 mm in diameter and 6.35 mm thick. The two windows were separated by a 6.35 mm thick rubber ring. This provided a space between the windows that could be used

for circulation of hot air to prevent condensation on the observation port. The hot air supplied by an external heater was admitted through a fitting on the left side of the aluminum support frame, circulated through small holes drilled in the rubber separation ring to the viewing windows and exhausted out the right side of the support frame. Figure 25 illustrates the details of the observation port support frame.

The observation port was held in place using six 6.5 mm long bolts secured to a tapered split aluminum flange. Again a vacuum seal was provided by the use of an "O" ring between the inner observation window and the Pyrex glass cross.

B. SUPPORT SYSTEMS

Three different support systems were required for the operation of the condensing chamber. These consisted of 1) the cooling water system, 2) the vacuum system and 3) the refrigeration system.

1. Cooling Water System

The purpose of the cooling water system was to remove heat from the test surface and the auxiliary condenser. The system consisted of a pump, condenser test section, flowmeter, auxiliary condenser, storage reservoir and associated tubing. Figure 1 schematically illustrates the cooling water system as a part of the apparatus schematic.

A 1/3 horse power Cole Parmer centrifigul pump was used to supply cooling water to the system and recirculate

water in the reservoir. Because of the low volumetric flow rate through the system it was necessary to recirculate the reservoir water to maintain a sufficient flow through the refrigeration cooling coil (evaporator).

The storage reservoir measuring 86.36 cm long, 33.02 cm wide and 30.48 cm deep was made of 0.635 mm thick stainless steel. Figure 26 shows a photograph of the storage reservoir. A 19.05 mm diameter galvanized bell mouth fitting, placed in the end of the reservoir, 63.5 mm from the bottom on the centerline, provided the suction inlet for the cooling water pump. At the outlet of the pump, a T-fitting was installed to divert cooling water back to the reservoir through a 12.7 mm diameter valve and pipe. The valve was used to control the cooling water flow rate through the system and recirculation line.

Connections between the various components of the cooling water system were made using 9.53 mm diameter thin wall copper tubing and Swagelok pressure fittings.

2. Vacuum System

Since the saturation temperature of steam is lower at pressures below atmospheric, it was advantageous to maintain a vacuum on the condensing chamber. This allowed for considerably lower operating temperatures resulting in a much smaller heating and refrigeration requirement. The primary components of the vacuum system were the vacuum pump, moisture separator, vacuum bleed valve and associated tubing and fittings.

A Duo Seal mechanical vacuum pump model 1405 was used to evacuate the condensing chamber. During operational runs this pump was found to provide reduced pressures of 103.0 mm Hg. absolute. Lower pressures, however, were possible.

Since the suction for the vacuum pump was located in the top end plate, moisture was pumped from the condensing chamber. To prevent damage to the vacuum pump a moisture separator was installed in the vacuum line. Steam and hot moist air from the condensing chamber entered a copper cylindrical air tight canister surrounded by an ice-water bath. Upon striking the cold walls of the copper canister, the moisture condensed out and accumulated in the bottom. The dry air then left the canister and flowed into the vacuum pump. Low pressure air inlet and outlet ports were also installed in the copper canister. Simply by closing the vacuum inlet and outlet valves and opening the low pressure air inlet and outlet valves, the moisture accumulated could be removed without disassembly of the moisture separator. Figure 27 illustrates the details of the moisture separator.

The vacuum in the condensing chamber was controlled by installing a small bleed valve between the moisture separator and the vacuum pump. Although quite sensitive, it was found that the pressure could be controlled extremely well using the bleed valve.

3. Refrigeration System

Since it was desired to use a closed cooling water loop during these tests, a method of removing heat absorbed by the cooling water in the test section and auxiliary condenser was needed. This was accomplished by using a 1/3 horsepower Tecumseh refrigeration system shown in Figure 28. This system consisted of a compressor, condenser, receiver, evaporator and thermostatic control valve.

The evaporator, installed in the storage reservoir, served as the heat exchanger removing heat from the cooling water. Heat removed from the cooling water was absorbed by the refrigerant (Freon 12) and rejected to the atmosphere at the condenser. The temperature in the storage reservoir was controlled by a Penn-Baso #A19ABC-4 thermostat. This device was temperature actuated by a sensor placed at the cooling water discharge side of the evaporator and was adjustable over the temperature range 10°C to 54°C.

C. INSTRUMENTATION

One of the most critical components of an experimental apparatus is the instrumentation. In the case of dropwise condensation, accuracy and sensitivity of measuring instruments is required because of the small temperature differences between the saturated vapor and the condensing surface temperature as well as between the cooling water inlet and outlet temperatures in the test section.

The instrumentation used in this experimental study is reviewed in the following paragraphs.

1. Temperature Measurement System

The measurement of various temperatures was attempted in two different ways. First, saturated vapor and cooling water temperatures were measured by the use of thermocouples. Second, the surface temperatures of the test surfaces were measured by thin film resistance thermometers. As described later, with the unsuccessful attempt at using the thin film resistance thermometer, an intrinsic thermocouple was finally chosen to measure the condensing surface temperature.

a. Thermocouples

Six 152.4 mm long, copper-constantan grounded junction thermocouples with 0.508 mm diameter stainless steel sheaths were used to measure the cooling water inlet and outlet temperatures in the test section. Two of the thermocouples were placed in the inlet tube 25.4 mm from the entrance and four thermocouples were inserted in a circular array in the cooling water outlet tube, 50.8 mm from the exit. Redundant thermocouples were used for comparison and to detect any existence of a temperature profile in the cooling water flow. In actual operation, it was found that this thermocouple system gave an excellent temperature indication as long as the flow rate was maintained below 0.042 kg/sec. At higher flow rates, the temperature readings became very erratic.

The saturation vapor temperature in the condensing chamber was measured using two 304.8 mm long, copper-constantan thermocouples with 3.18 mm diameter stainless steel sheaths. Penetration into the condensing chamber

was made through the top end plate using Swagelok pressure fittings with teflon seals. Figure 24 gives the detailed location of each fitting. An attempt was made to locate one thermocouple as close to the test surface as possible while using the other thermocouple in the adjacent area as a check.

A Hewlett Packard Model 2010 C Data Acquisition System was used to monitor and record the output from the thermocouples. This instrument sensed the voltage from each thermocouple and converted the signal to a digital display. It automatically scanned each thermocouple at a designated interval and presented the data on a digital recorder.

b. Thin Film Resistance Thermometers

One of the major stumbling blocks in this thesis was to find a method of measuring the surface temperature of the test surfaces while at the same time not affecting the rate of heat transfer or condensate drop formation. It was also necessary to find a method that was compatible with the very thin test surfaces being used.

In the experimental work conducted by Hannemann and Mikic [11], a thin film thermometer was used to measure surface temperature. A similar method was therefore developed and constructed for this thesis. The thin film thermometer used is shown in Figure 18. The steam-side of the stainless steel test surfaces were first polished to a mirror finish, using a one micron polishing wheel. Each surface was then coated at Varian Corp. with a thin insulating

layer of (tri)silicon (tetra)nitride (Si_3N_4), 0.001 mm thick, using a sputtering technique. The surface was then coated with a 0.0001 mm thick layer of titanium. A meander pattern was then generated in the titanium, using a photographic etching process. Appendix A lists in detail the procedures used in this photographic etching process. After the titanium was etched, an additional layer of Si_3N_4 was applied to the surface followed by a 0.0005 mm thick layer of gold to promote the dropwise condensation process. Figure 18 also shows a cross sectional view through the disk indicating the various layers and their respective thicknesses. Figure 29 is an actual photograph of the test surface, showing the etched titanium meander thermometer.

Figure 30 details the test surface installation and hook-up of the resistance measuring equipment. Thin copper wires (0.64 mm in diameter) were inserted through the walls of the nylon test section and allowed to protrude out 2.0 mm on each side of the test surface. An air tight seal was then provided by epoxying the wires in place. Short lengths (approximately 5.0 mm) of 0.15 mm diameter fine copper wire were then soldered to the ends of the protruding wires. The opposite ends of the fine copper wires were attached to the titanium terminals of the thin film thermometer on the test surface using a conductive copper paint. The terminals were then coated with epoxy to provide the strength needed to hold the copper wires in place. Since any moisture present would short out the resistance grid, all exposed wiring was coated with a waterproof insulating

varnish. This system of installation and hook-up provided for easy removal and installation of test surfaces. The two leads from the resistance thermometer were connected to a high precision Rosemount Commutating Bridge Model 920 A to measure changes in electrical resistance.

c. Intrinsic Thermocouple

When the attempt to calibrate the thin film resistance thermometer failed, as described in Appendix B, another method had to be found to measure the temperature on the condensing surface. Because of the simplicity of attachment to the condensing surface and reliability of output, the decision was made to use a copper-constantan intrinsic thermocouple.

Intrinsic thermocouple leads are not connected at a point junction but are joined at two different points with the attached surface completing the electrical circuit. This tends to give more of an average surface temperature than with a conventional, extrinsic thermocouple.

A 0.51 mm thick stainless steel test surface polished to a one micron mirror finish was used as the condensing surface. Using a Unitek 1065 Weldmatic tack welder, 0.254 mm copper-constantan thermocouple leads were attached to the test surface 15.9 mm apart. With the surface thickness of 0.51 mm it was necessary to use 40.0 watt-second welding power to attach the leads securely.

The wires originally installed in the nylon test section walls for the thin film resistance thermometer

were removed and replaced with one copper and one constantan lead. The leads were then epoxied in place to provide a vacuum seal, allowing 2.0 mm to protrude out on each side of the test surface. Similar to the resistance thermometer, the copper-constantan thermocouple leads were soldered to their respective terminals.

The Hewlett Packard Model 2010 C Data Acquisition System was again used to monitor and record the output from the intrinsic thermocouple.

A Hewlett Packard 7100 B Strip Chart Recorder was also used to record the intrinsic thermocouple output since it was expected that a dynamic temperature variation would most likely exist on the condensing surface.

2. Flowmeter

The flow rate of the cooling water through the test section was measured using a Fischer and Porter Precision Bore Flowrator, Model 10A3565A, Tube No. FP-1/2-27-G-10/83, with a maximum flow rate of 0.070 kg/s of liquid with a specific gravity of 1.0. Appendix B provides the details of the calibration procedure for the flowmeter.

Figures 1 and 2 illustrate the location of the flowmeter with respect to the other apparatus.

3. Mercury Manometer

Measurement of the pressure inside the condensing chamber was accomplished by using a U-tube mercury manometer which was marked off in millimeters. This manometer was connected with a vacuum hose to a Swagelok pressure

fitting on the top end plate of the condenser. The location of the manometer can be seen in Figures 1 and 2.

III. EXPERIMENTAL PROCEDURES

A. TEST SURFACE PREPARATION

In order to obtain reliable dropwise condensation, it was necessary to coat the surface with a promoter. One of the chemical promoters that was used quite successfully by Morgan [14] was a mixture of one percent by weight n-octadecyl mercaptan in octanoic acid. Because of its availability and excellent promoting capability, octadecyl mercaptan was used for this experiment.

After installing the test surface in the test section, the following procedure was used to apply the promoter to the stainless steel surface:

1. The surface was carefully swabbed and rinsed with ethyl alcohol to remove any surface contamination. It was then allowed to dry in air.

2. Using a cotton swab, the surface was then wiped with the promoter, ensuring complete coverage.

3. Excess promoter was then washed off the surface with distilled water.

Immediately following the application of the promoter the test section was installed in the condensing chamber and the experimental startup operation commenced.

B. STARTUP AND OPERATION

The following procedures were used to startup and operate the experimental apparatus. It should be noted that

experimentation requiring a variation of different parameters may require some change in the operating procedures although the basic startup will still be the same.

1. Approximately 24 hours prior to an experimental run, the data acquisition system and electronic ice point reference junction were turned on. This allowed the electronic equipment to begin warming up to a steady state.

2. The cooling water reservoir was filled with distilled water, covering the refrigeration cooling coil.

3. The condensing chamber was filled with distilled water to approximately five centimeters above the immersion heaters. This was accomplished by removing the thermocouple fitting in the top end plate and using a small funnel.

4. The low pressure air supply to the air heater was turned on, and the variable power supply was set to 30 percent. This heater setting provided a sufficient heat supply to keep the observation port clear of moisture.

5. The cooling water system was prepared by opening the cooling water reservoir recirculation valve, closing the auxiliary condenser bypass valve, and opening the cooling water flowrate valve.

6. The cooling water pump was started and the cooling water flowrate valve was adjusted to allow for a 60 percent (0.042 kg/sec) flowrate on the flowmeter.

7. The moisture separator vacuum flask was filled with crushed ice and the separator was assembled. The LP air

inlet and outlet valves were closed and the inlet and outlet vacuum valves were opened.

8. The vacuum bleed valve was opened and the vacuum pump was started. The bleed valve was throttled until a vacuum of approximately 625 mm Hg was obtained in the condensing chamber.

9. The variable power supply to the immersion heaters was then set to 35 percent (450 watts) and the system was allowed to come to an equilibrium temperature, making adjustments as necessary.

10. After equilibrium temperatures had been reached, the refrigeration system was turned on and the cooling water thermostat was adjusted to the desired temperature. If it was necessary to increase the temperature of the cooling water, immersion heaters installed in the reservoir were used.

C. HEAT TRANSFER DATA REDUCTION

Since the heat flux was controlled by the temperature of the cooling water on the back side of test surface, the decision was made to vary the cooling water temperature through a specified range while holding all other parameters fixed. The temperature was varied between 10°C and 55°F in increments of 2.8°C.

1. Heat Flux Determination

Heat flux through the test surface was determined using the equation

$$q/A = \frac{\dot{m}_{cw} C_p \Delta T_{cw}}{A} \quad (1)$$

where

\dot{m}_{cw} = cooling water mass flow rate from flowmeter (kg/s)

C_p = specific heat of the cooling water at the average temperature (kJ/kg - °C)

ΔT_{cw} = cooling water outlet minus inlet temperature difference from thermocouples (°C)

A = surface area of the test surface (m²)

2. Temperature Determination

The temperature of the cooling water into the test section was obtained by inputting the two thermocouple values from the data acquisition system into the calibration program. The two output values from the program were then arithmetically averaged and this value was used for $T_{cw\text{in}}$. The cooling water outlet temperature was determined in the same manner except that four thermocouples were used to obtain the arithmetic average for $T_{cw\text{out}}$.

The saturated vapor temperature was determined from the arithmetic average of the two vapor space thermocouples read on the data acquisition system. Again the output data was converted using the calibration program.

The condensing surface temperature was obtained by reading the output value of the intrinsic thermocouple. Since the output from this thermocouple was erratic, between 15 and 20 readings were taken and then arithmetically averaged to give one output value. This value was entered into the calibration program with the output temperature being

used as T_{wall} . Figure 31 is an actual trace of the intrinsic thermocouple output at a ΔT of 6.97°C showing the erratic condensing surface temperature.

3. Heat Transfer Coefficient Determination

The heat transfer coefficient on the steam side of the condensing surface was determined from Newton's Law of Cooling

$$\bar{h}_{ss} = \frac{q/A}{T_{\text{vap}} - T_{\text{wall}}} \quad (2)$$

where

q/A = heat flux obtained from equation (1) ($\frac{\text{kw}}{\text{m}^2}$).

T_{vap} = temperature of the saturated vapor from the vapor space thermocouples ($^{\circ}\text{C}$).

T_{wall} = temperature of condensing surface from intrinsic thermocouple ($^{\circ}\text{C}$).

IV. PRESENTATION AND DISCUSSION OF RESULTS

A. GENERAL

One experimental run was conducted using a 0.5 mm thick stainless steel condensing surface. Data was obtained at 14 different cooling water temperatures. The data was reduced and the results are listed in Table 2. The results are also presented graphically in Figure 32 which compares the present data with that of Takeyama and Shimizu [8].

B. DROPWISE CONDENSATION RESULTS

The data from the single experimental run was reduced and displayed graphically as can be seen in Figure 32. There are several different points that should be made about this graphical data. The first thing to notice is the shape of the curve formed by the present data. The data takes a shape similar to the Takeyama [8] condensing curve also shown in Figure 32. This result verifies the existence of such a condensing curve and shows that the present experimental apparatus can be utilized to obtain such a curve.

It was also found during the current research that a very unstable region was encountered when high temperature differences were created. Takeyama and Shimizu [8] also encountered this unstable region which is indicated by the existence of a hysteresis loop in the upper right hand portion of Figure 32. In the current work, the instability

was indicated by very erratic condensing surface temperatures. (See Figure 31.)

The second point which should be noticed about Figure 32 is the existence of a maximum heat flux. For the present data this maximum occurred at a temperature difference of approximately five degrees Celsius. This result indicates that during dropwise condensation there does exist a temperature difference past which increasing the vapor temperature or decreasing the cooling water temperature will actually decrease the heat transfer rate for a specific tube wall thickness and material.

The third point to notice in Figure 32 is the location of the maximum heat flux for the stainless steel surface compared to the results of the copper test surface. The present data for stainless steel, shows both a drop in heat flux and a shift to a lower $T_{\text{vap}} - T_{\text{wall}}$ at the maximum heat flux. This very strongly shows the effect of condensing surface thermal conductivity on maximum heat flux.

Table 2 indicates the range of steam side heat transfer coefficients obtained for the different $T_{\text{vap}} - T_{\text{wall}}$. It should be noted that for the lower temperature differences, heat transfer coefficients up to $165900 \text{ w/m}^2\text{°C}$ ($29760 \frac{\text{BTU}}{\text{HR-FT}^2\text{-°F}}$) were obtained. Even though a 25 percent uncertainty exists in the heat transfer coefficient, these high values are still characteristic of dropwise condensation. These values decreased rapidly as $T_{\text{vap}} - T_{\text{wall}}$ was increased.

During the entire experimental run which was approximately eleven hours in length, the experimental apparatus operated exactly as designed. The refrigeration system also worked very well in controlling the cooling water temperature. It is suggested that the refrigeration system be used only for very high $T_{\text{vap}} - T_{\text{wall}}$ since the high cooling water temperatures needed for a low $T_{\text{vap}} - T_{\text{wall}}$ were not compatible with the refrigeration system. This was shown by a drastic rise in the temperature of the refrigeration compressor. The immersion heaters installed in the cooling water reservoir can be used to obtain the low temperature differences.

C. THIN FILM RESISTANCE THERMOMETER

After the attempt to calibrate the thin film resistance thermometer failed, several electrical continuity checks were made on the device. It was found from these checks that continuity existed between the stainless steel, titanium and gold which were intended to be electrically insulated from each other. These parallel resistance paths are thought to be the reason for the inability to calibrate the device. The reason for the silicon nitride dielectric breakdown is unknown. There is a possibility that during the cooling down period following the sputtering of the silicon nitride that cracks formed in the dielectric. Even though a continuity check between the silicon nitride and the stainless steel substrate indicated a very high electrical resistance, cracks still could have been present.

An attempt to microscopically examine the silicon nitride was not possible due to the unavailability of the scanning electron microscope during these procedures.

V. CONCLUSIONS AND RECOMMENDATIONS

A. CONCLUSIONS

1. An experimental apparatus has been designed and constructed that allows the testing of condensing surfaces of various thickness. The equipment also has the ability to verify the Takeyama and Shimizu [8] condensing curve for materials of various thermal conductivity.

2. There does exist a condensing curve similar in shape and characteristics to the boiling curve. This curve appears to be affected by the thermal conductivity of the condensing surface.

3. A thin film resistance thermometer should be used to obtain the average temperature of the condensing surface. Thermocouples placed on the condensing surface distort the dropwise condensation process and give a very localized, erratic surface temperature.

B. RECOMMENDATIONS FOR FURTHER WORK

1. Experimentally examine the condensing curve, paying special attention to very high and very low temperature differences between saturation temperature and condensing surface temperature.

2. Make a concerted effort to have a thin film resistance thermometer commercially built.

3. Experimentally construct condensing curves for condensing surfaces of different thickness and attempt to determine the effect of the condensing surface thickness on the heat transfer coefficient for dropwise condensation.

APPENDIX A

PHOTOGRAPHIC ETCHING PROCEDURES

The procedures used to generate the meander pattern in the titanium layer on the test surface were very similar to the photographic etching techniques used in the production of printed circuit boards.

First the test surface, coated with a layer of silicon nitride and titanium, was cleaned with a cotton swab saturated with ethyl alcohol. The surface was then rinsed with the alcohol and allowed to dry thoroughly. Next the test surface was dipped in a solution of 50 percent 1.0 centistoke KTI 752 photo-resist and 50 percent zylene. After removing the excess solution by a shaking motion the test surface was allowed to soft bake in an oven for 25 minutes at 90°C. Upon completion of baking the test disc was inserted into a special glass container designed to hold a photographic negative mask in place over the test surface. The photographic mask, patterned after the meander grid to be etched onto the test surface, allowed ultraviolet light to selectively expose the photo-resist. After a ten-minute exposure to the ultraviolet light the test disc was developed for 25 seconds in a bath of zylene to remove the unexposed portions of the photo-resist. At this point the test disc was allowed to hard bake in an oven for 25 minutes at 140°C. This second bake insured the removal of the developing chemical and strengthened the adhesion of

the photo-resist to the surface. Upon completion of the hard bake actual acid etching was ready to proceed.

After considerable research it was found that very little information existed on the subject of titanium etching. The Metals Handbook [15] listed mixtures of hydrofluoric and nitric acids as being used for macro-etching of titanium. Because of the highly corrosive nature of hydrofluoric acid, the decision was made to use a weak solution containing two percent hydrofluoric acid, two percent nitric acid and 96 percent water. It was felt that this solution would give more control over the actual etching process.

Each test disc was immersed in the etching solution for 15 to 20 seconds or until a dark blue color appeared on the surface. The color change indicated the removal of the titanium and the chemical reaction of the etchant with the silicon nitride. At the end of the time period the disc was immediately dipped in fresh water to stop the etching reaction.

The remaining photo-resist was removed from the test surface by dipping in a bath of zylene for approximately two minutes and then gently scrubbing with a saturated cotton swab. This completely cleaned the surface leaving only the etched titanium meander grid pattern remaining.

APPENDIX B

CALIBRATION OF INSTRUMENTS

1. Thermocouples

One of the critical areas in experimental work on dropwise condensation is the measurement of temperature. Because of the small temperature difference between the saturated vapor and the condensing surface in the condensing chamber, and the cooling water inlet and outlet temperatures in the test section, it is essential that the thermocouple calibration be as accurate as possible.

To achieve the necessary accuracy for this work the eight thermocouples used, plus two standby thermocouples, were calibrated using a Rosemount Engineering Company Model 913A Variable Temperature Oil Bath. All ten thermocouples were suspended at once into the oil bath with their leads connected to the Hewlett Packard Data Acquisition System.

The temperature of the oil bath was measured using a Platinum Resistance Thermometer connected to a high precision Rosemount Commutating Bridge Model 920A. This system which provided an accuracy of $\pm 0.002^{\circ}\text{C}$ was used as the standard for the calibration.

After allowing a 24-hour warmup period for the Hewlett Packard Data System, the calibration was commenced for a temperature range from 0°C to 100°C in increments of 5°C . A nominal temperature was set for the oil bath which was then allowed to settle for ten minutes prior to any reading

being taken. The digital recorder was then actuated on the Data Acquisition System and allowed to scan and record the millivolt output for each of the ten thermocouples. Five continuous runs were made for each thermocouple at each temperature and were averaged to give one output reading. The standard temperature from the Platinum Resistance Thermometer was then read on the Commutating Bridge in ohms and converted directly to degrees centigrade using the conversion tables supplied by the thermometer manufacturer.

A computer program utilizing the IBM Scientific Subroutine Library subroutine INTRPL was used to convert millivolt reading from the thermocouples to degrees centigrade. This subroutine utilized a piecewise cubic interpolation scheme through the calibration points to provide a smooth calibration curve.

2. Thin Film Resistance Thermometer

As mentioned earlier, because of the high accuracy needed in measuring the temperature of the condensing surface, the Rosemount variable temperature bath was used in an attempt to calibrate the thin film resistance thermometer. It was necessary to replace the silicone oil in the temperature bath with distilled water so the test surface would not become contaminated. A Platinum Resistance Thermometer was again used as the standard for the temperature in the calibration bath.

Since the thin film resistance thermometer was newly constructed and untested, several initial temperature points

were checked for linearity and repeatability prior to calibrating. Measurements were taken at 31°C, 42°C and 93°C. The titanium resistance change measured on the commutating bridge was neither linear nor repeatable. Several different runs were made at various other temperatures with even more erratic results. For the temperature range from 30°C to 90°C, the resistance of the thermometer varied erratically in the range from 100 to 200 ohms.

A second test disk was installed in the test section and another calibration run attempted. Again as with the case of the first resistance thermometer, very erratic and non-repeatable data was obtained. For a temperature range from 30°C to 55°C, the resistance of this second thermometer varied erratically from 50 to 100 ohms.

At this point it was felt that any further attempt at calibrating the resistance thermometers would be futile.

3. Intrinsic Thermocouple

Calibration procedures for the intrinsic condensing surface thermocouple were identical to those used for the steam vapor and cooling water thermocouples except the calibration bath contained distilled water instead of silicon oil to avoid test surface contamination.

A calibration curve was again reduced from the data by a computer program utilizing the IBM subroutine INTRPL.

4. Flowmeter

To measure the flowrate of the cooling water through the test section, a constant cross section Precision Bore Flowrator Tube FP-1/2-27-G-10/83 with a maximum flowrate of 4.23

kilograms per minute was used. Since the flowrate of the cooling water was an integral part of the calculation for the heat transfer rate, it was necessary to calibrate the flowmeter as accurately as possible.

The calibration was performed over the entire scale of the flowmeter in increments of 10 percent. A Toledo Scale with a capacity of 0-90 pounds marked in increments of 0.1 pound was used to measure the amount of water through the flowmeter. The time needed to fill a container resting on the scale was measured by a stop watch marked in increments of 0.2 second. The weight of the water accumulated in the container at each step was then divided by the time to give the mass flow rate of the water. Table 1 gives a summary of the calibration of the flowmeter.

APPENDIX C

UNCERTAINTY ANALYSIS

The procedures used in determining the uncertainty of the calculations for this experimental work were from a method proposed by Kline and McClintock [16] for Single-Sample experiments. In this method if the result, R , of a calculation is a function of n independent variables V_1, \dots, V_n , then the uncertainty in R , W_R , is given by the following relation:

$$W_R = \left[\left(\frac{\partial R}{\partial V_1} W_1 \right)^2 + \left(\frac{\partial R}{\partial V_2} W_2 \right)^2 + \dots + \left(\frac{\partial R}{\partial V_n} W_n \right)^2 \right]^{1/2} \quad (C-1)$$

where W_1, \dots, W_n are the uncertainties in each of the independent variables V_1, \dots, V_n .

Equation (C-1) can be simplified by dividing through by the result, nondimensionalizing the terms and reducing the uncertainty to a percentage. Accomplishing this, equation (C-1) then becomes

$$\frac{W_R}{R} = \left[\left(\frac{1}{R} \frac{\partial R}{\partial V_1} W_1 \right)^2 + \left(\frac{1}{R} \frac{\partial R}{\partial V_2} W_2 \right)^2 + \dots + \left(\frac{1}{R} \frac{\partial R}{\partial V_n} W_n \right)^2 \right]^{1/2} \quad (C-2)$$

In this work the following relationships were used in determining the final results:

$$q/A = \frac{\dot{m}_{cw} C_p \Delta T_{cw}}{A} \quad (C-3)$$

$$\bar{h}_{ss} = \frac{q/A}{(T_{vap} - T_w)} \quad (C-4)$$

Using equation (C-2), equations (C-3) and (C-4) take the following form.

$$\frac{W_{g/A}}{g/A} = \left[\left(\frac{W_{\dot{m}_{cw}}}{\dot{m}_{cw}} \right)^2 + \left(\frac{W_{C_P}}{C_P} \right)^2 + \left(\frac{W_{\Delta T_{CW}}}{\Delta T_{CW}} \right)^2 + \left(-\frac{W_A}{A} \right)^2 \right]^{1/2} \quad (C-5)$$

$$\frac{W_{\dot{h}_{ss}}}{\dot{h}_{ss}} = \left[\left(\frac{W_{g/A}}{g/A} \right)^2 + \left(-\frac{W_{(T_{vap}-T_w)}}{(T_{vap}-T_w)} \right)^2 \right]^{1/2} \quad (C-6)$$

Using the two equations above, the uncertainties for one run were calculated. The results from these calculations are shown in Table 2.

The uncertainties for the different known parameters needed in equations C-5 and C-6 are described below.

The uncertainty in the mass flow rate of the cooling water, \dot{m}_{cw} , was associated primarily with the calibration of the flowmeter. Since the cooling water pump produced a constant output head pressure, very little fluctuation occurred in the cooling water flow. Appendix B describes the calibration of flowmeter which is outlined briefly below:

$$\dot{m}_{cw} = \frac{W}{t} \frac{g_c}{g} = \frac{m}{t} \quad (g=g_c \text{ at sea level})$$

where

W is in lbf,
m is in lbm, and
t is in seconds.

Using

$$W_m = 0.1 \text{ lbm}, \\ W_t = 0.2 \text{ sec}$$

gives

$$\frac{W_{\dot{m}_{cw}}}{\dot{m}_{cw}} = \left[\left(\frac{0.1}{m} \right)^2 + \left(-\frac{0.2}{t} \right)^2 \right]^{1/2} \quad (C-7)$$

The specific heat, C_p , is taken to have an uncertainty of 0.001 kJ/kg - °C.

The uncertainty in the condensing surface area, A , is due to the measurement of the disc active condensing diameter using a pair of calipers. The calipers were marked in increments of 0.001 in. (0.0254 mm).

The area is calculated from

$$A = \pi \left(\frac{d}{2} \right)^2$$

where the diameter, d , is in millimeters. Again using equation (C-2) gives:

$$\frac{W_A}{A} = \left[\left(\frac{0.0254}{31.60} \right)^2 + \left(\frac{0.0254}{31.60} \right)^2 \right]^{1/2} = .001$$

The uncertainty in the cooling water temperature difference, ΔT_{cw} , was a combination of 1) data acquisition system accuracy, 2) thermocouple calibration, 3) temperature measurement errors and 4) fluctuation of digital data output.

The Hewlett Packard 2010 C is readable to ± 0.001 millivolt which corresponds to 0.002°C.

The uncertainty introduced by the thermocouple calibration can be separated into temperature measurement and data reduction. The calibration system provided an accuracy of $\pm 0.002^\circ\text{C}$. Since the computer program used to interpolate the calibration curve piecewise fitted third order polynomials between the given calibration points there would not be any uncertainty greater than that of the given calibration points. Therefore the uncertainty of the data

reduction would also be $\pm 0.002^{\circ}\text{C}$ giving a total thermocouple calibration uncertainty of $\pm 0.004^{\circ}\text{C}$.

Since the nylon cooling water inlet and outlet tubes had such a low thermal conductivity the inside walls of the flow channels were assumed to be at the same temperature as the cooling water. Similarly conduction was neglected since all of the 0.508 mm diameter thermocouples were installed at least 25.0 mm into the cooling water flow.

During the experimental runs fluctuations of ± 0.001 millivolts were found in the cooling water digital data. This variation corresponded to a $\pm 0.024^{\circ}\text{C}$ uncertainty.

Adding the four different uncertainties together, the cooling water temperature difference was $\pm 0.03^{\circ}\text{C}$.

The uncertainty in the steam saturation temperature, T_{vap} , was made up of the same errors as the cooling water temperature difference. The data acquisition system accuracy and thermocouple calibration error were identical. Because of condensing chamber insulation and long thermocouple runs, radiation and conduction error were again neglected. The fluctuation of the digital output was found to be $\pm 0.002\text{mv}$ corresponding to $\pm 0.046^{\circ}\text{C}$. Totaling the uncertainties gave an error of $\pm 0.052^{\circ}\text{C}$ for the steam saturation temperature.

The wall temperature, T_w , of the condensing surface was obtained from the intrinsic thermocouple. The data acquisition system and thermocouple calibration errors are the same as for the steam vapor and cooling water thermocouples.

Temperature measurement errors were taken to be $\pm 0.05^{\circ}\text{C}$ which is due to any conduction through the thermocouple leads. The leads were installed very close to the condensing surface so very little effect would result from conductive errors. The fluctuation of digital data output was found to provide the largest amount of error. For low temperature differences the fluctuations were approximately ± 0.013 which corresponds to 0.29°C . As the temperature difference increased the temperature fluctuations become much greater. For large ΔT ± 0.13 millivolts corresponded to an uncertainty of $\pm 2.9^{\circ}\text{C}$. As can be seen any error in the intrinsic thermocouple was due to the fluctuations in digital data output.

TABLE I

FLOWMETER CALIBRATION SUMMARY

Percent of Maximum Flow	Mass Flow Rate	
	(lbm/sec)	(kg/sec)
10	0.014	0.006
20	0.030	0.014
30	0.045	0.020
40	0.061	0.028
50	0.077	0.035
60	0.092	0.042
70	0.110	0.050
80	0.124	0.056
90	0.138	0.063
100	0.154	0.070

TABLE II

DATA CALCULATIONS WITH UNCERTAINTY LIMITS

Nominal C.W.Temp.(°C)	155.00	52.00	49.20	46.40	43.60	40.80	38.00	35.20	32.40	29.60	26.80	27.2	15.6	10.00
T _{cwin} (°C)	51.51	49.99	48.26	49.93	41.97	39.40	36.68	33.66	30.93	27.79	25.37	20.38	14.80	10.39
W _{Tcwin} (°C)	0.03	0.03	0.03	0.03	0.03	0.03	0.03	0.03	0.03	0.03	0.03	0.03	0.03	0.03
T _{cwout} (°C)	52.13	50.66	49.01	44.74	42.83	40.35	37.62	34.61	31.89	28.72	26.27	21.23	15.43	11.13
W _{Tcwow} (°C)	0.03	0.03	0.03	0.03	0.03	0.03	0.03	0.03	0.03	0.03	0.03	0.03	0.03	0.03
ΔT _{cw} (°C)	0.62	0.67	0.75	0.82	0.86	0.95	0.94	0.96	0.96	0.93	0.90	0.85	0.63	0.74
W _{ΔTcw} (°C)	0.03	0.03	0.03	0.03	0.03	0.03	0.03	0.03	0.03	0.03	0.03	0.03	0.03	0.03
m _{cw} (kg/sec)	0.041	0.041	0.41	0.41	0.41	0.41	0.41	0.41	0.41	0.41	0.41	0.41	0.041	0.041
W _{mew} (kg/sec)	0.001	0.001	0.001	0.001	0.001	0.001	0.001	0.001	0.001	0.001	0.001	0.001	0.001	0.001
q/A(kW/m ²)	165.9	178.8	200.2	220.5	226.8	255.0	248.8	255.5	256.7	246.1	249.6	229.8	169.9	196.9
W _q /A(kW/m ²)	8.99	9.12	9.38	9.70	9.67	11.93	10.00	10.13	10.18	9.95	10.31	9.86	9.09	9.32
T _{vap} (°C)	59.81	59.43	59.89	59.51	59.55	59.31	58.80	58.88	59.18	58.35	57.98	57.68	56.24	56.41
W _{Tvap} (°C)	0.05	0.05	0.05	0.05	0.05	0.05	0.05	0.05	0.05	0.05	0.05	0.05	0.05	0.05
T _{wall} (°C)	58.81	58.36	58.13	57.26	56.56	55.66	54.53	53.15	52.21	50.07	46.92	43.06	31.10	33.30
W _{Twall} (°C)	0.29	0.49	0.69	0.89	1.09	1.29	1.49	1.69	1.89	2.10	2.30	2.50	2.70	2.90
T _{v-Tw} (°C)	1.00	1.07	1.76	2.25	2.99	3.65	4.27	5.73	6.97	8.28	11.06	14.62	25.14	23.11
W _{Tv-Tw} (°C)	0.29	0.49	0.69	0.89	1.09	1.29	1.49	1.69	1.89	2.10	2.30	2.50	2.70	2.90
h _{ss} (kW/m ² °C)	165.9	167.2	113.8	97.98	75.85	69.85	58.28	44.59	36.83	29.72	22.57	15.72	6.76	8.52
W _{hss} (kW/m ² °C)	48.9	77.0	44.9	38.9	27.8	24.9	20.5	13.3	10.1	7.63	4.78	2.77	0.81	1.14

$$A = 641.03 \text{ mm}^2$$

$$C_{pcw} = 4.179 \text{ kJ/kg-}^\circ\text{C}$$

$$W_A = 0.64 \text{ mm}^2$$

$$W_{C_{pcw}} = 0.001 \text{ kJ/kg-}^\circ\text{C}$$

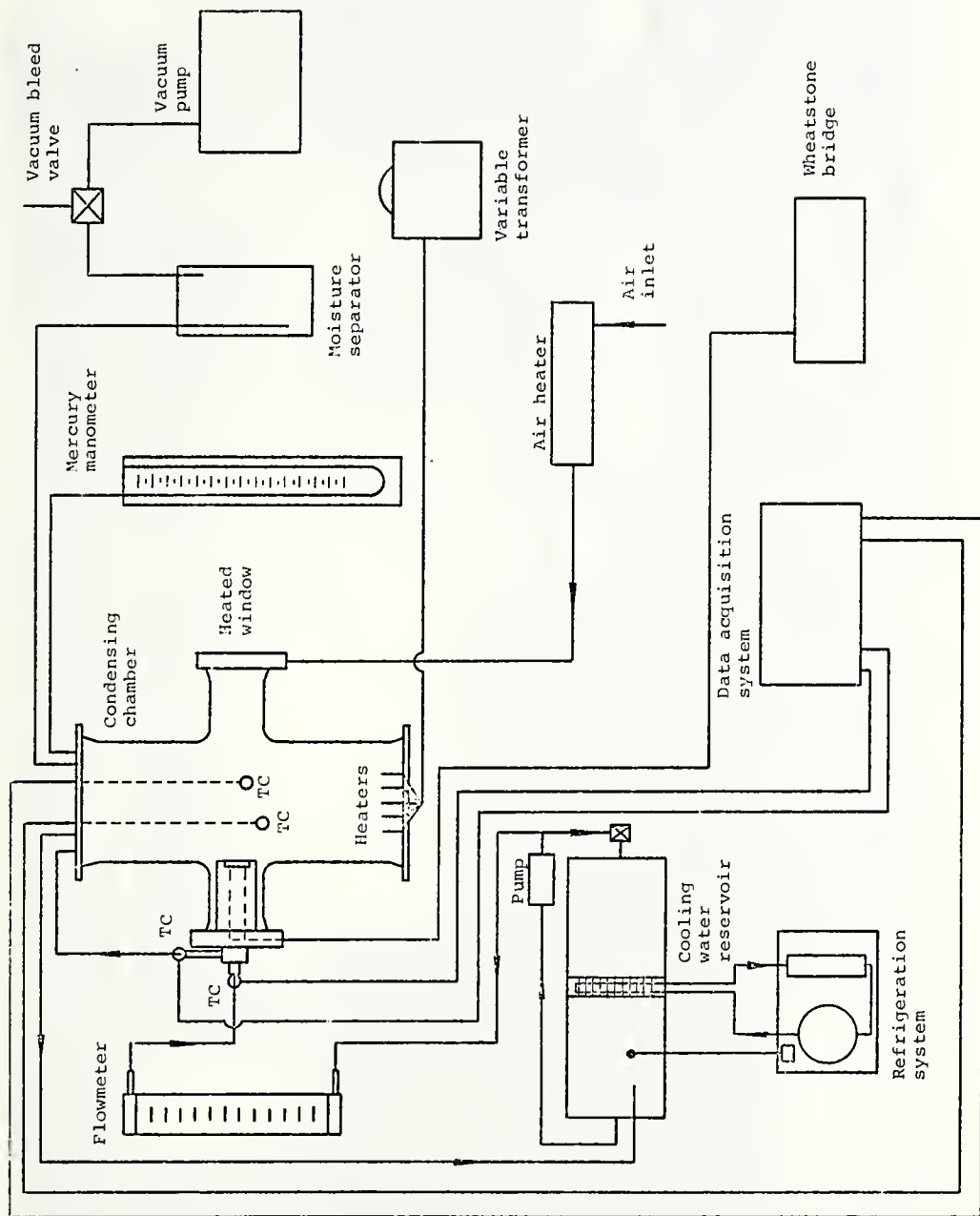


Figure 1 - Schematic Drawing of Experimental Apparatus

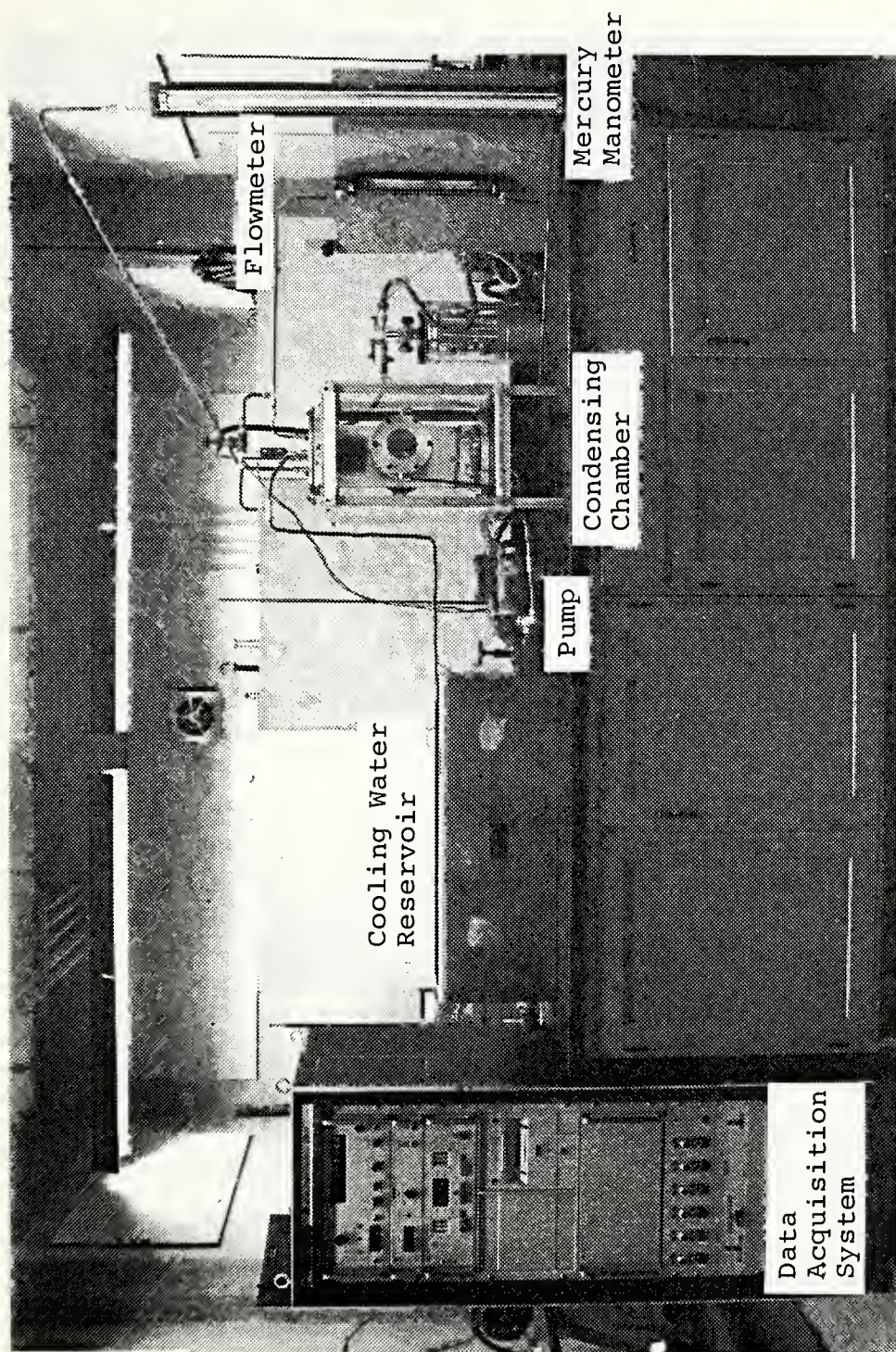


Figure 2 - Photographic Front View of Experimental Apparatus

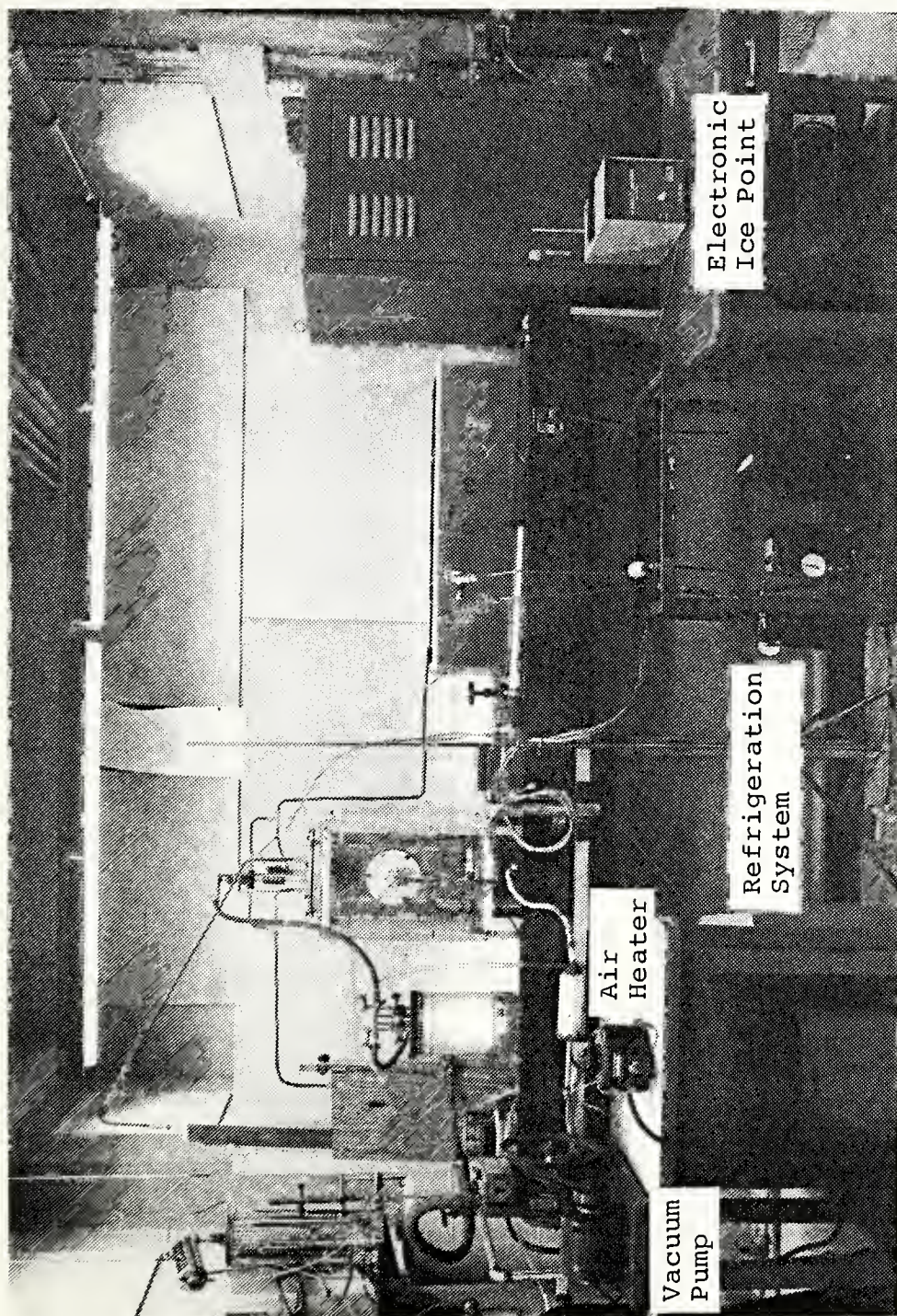


Figure 3 - Photographic Rear View of Experimental Apparatus

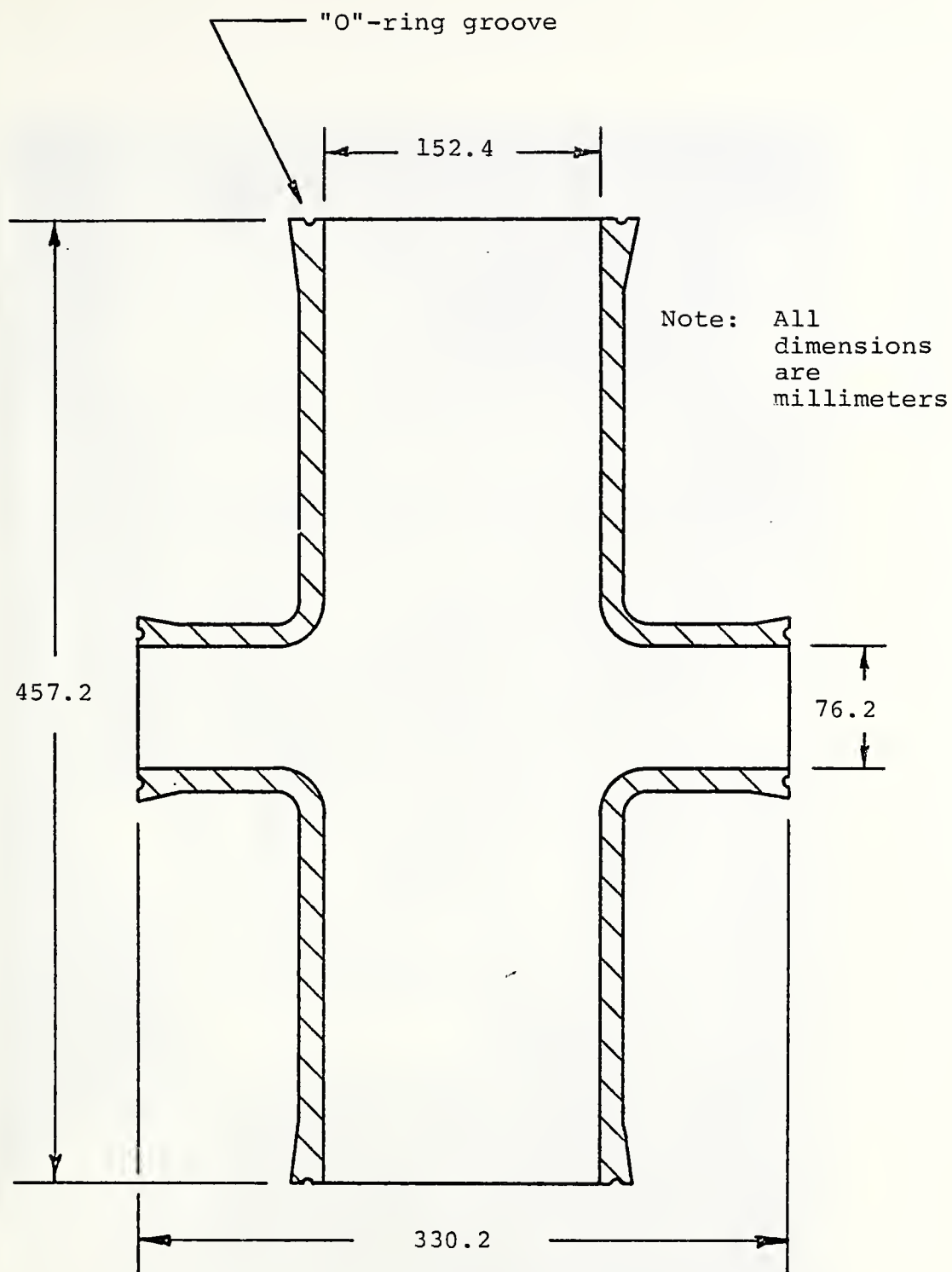


Figure 4 - Details of Pyrex Glass Cross

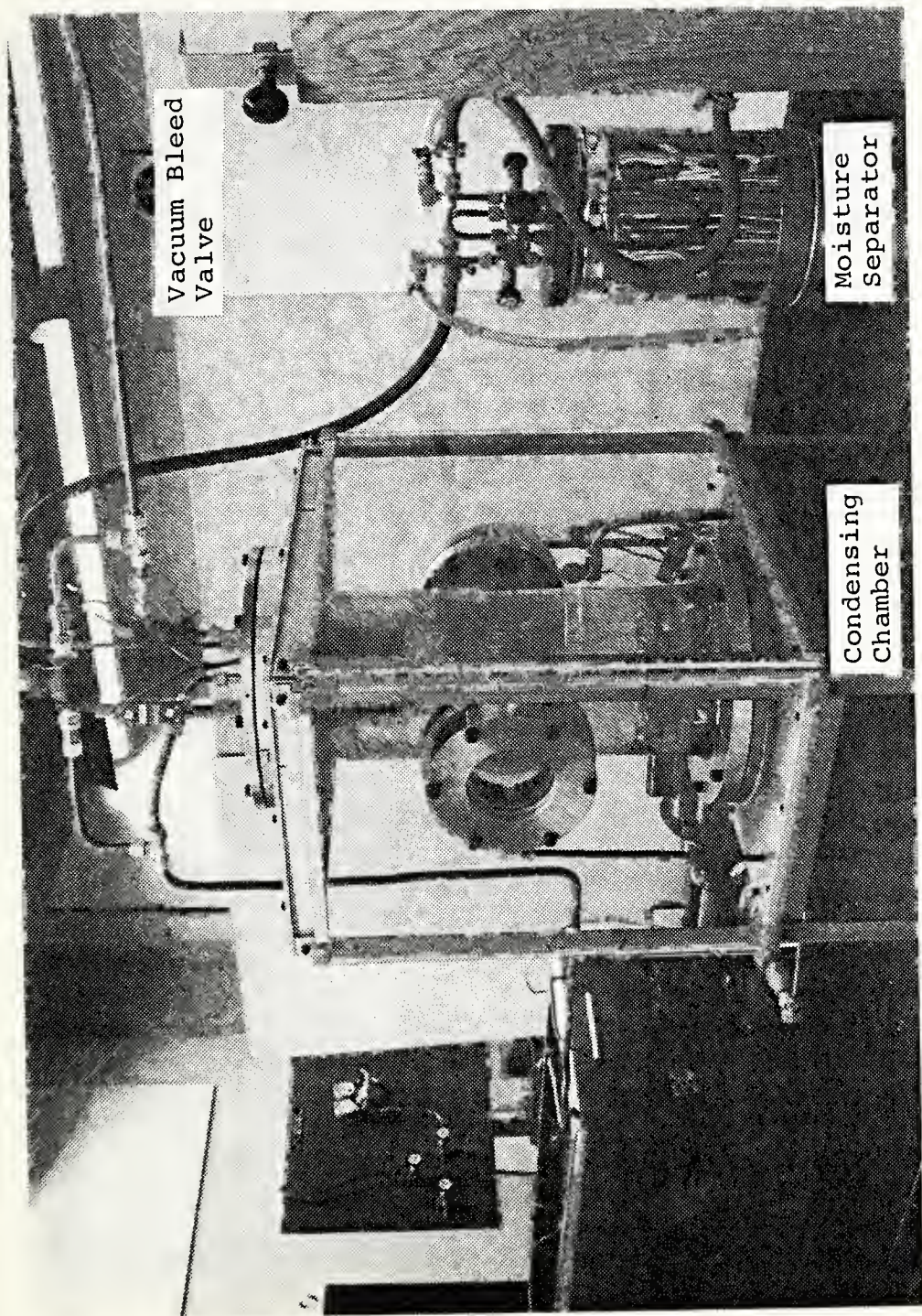


Figure 5 - Photograph of the Front, Right Side of the Condensing Chamber

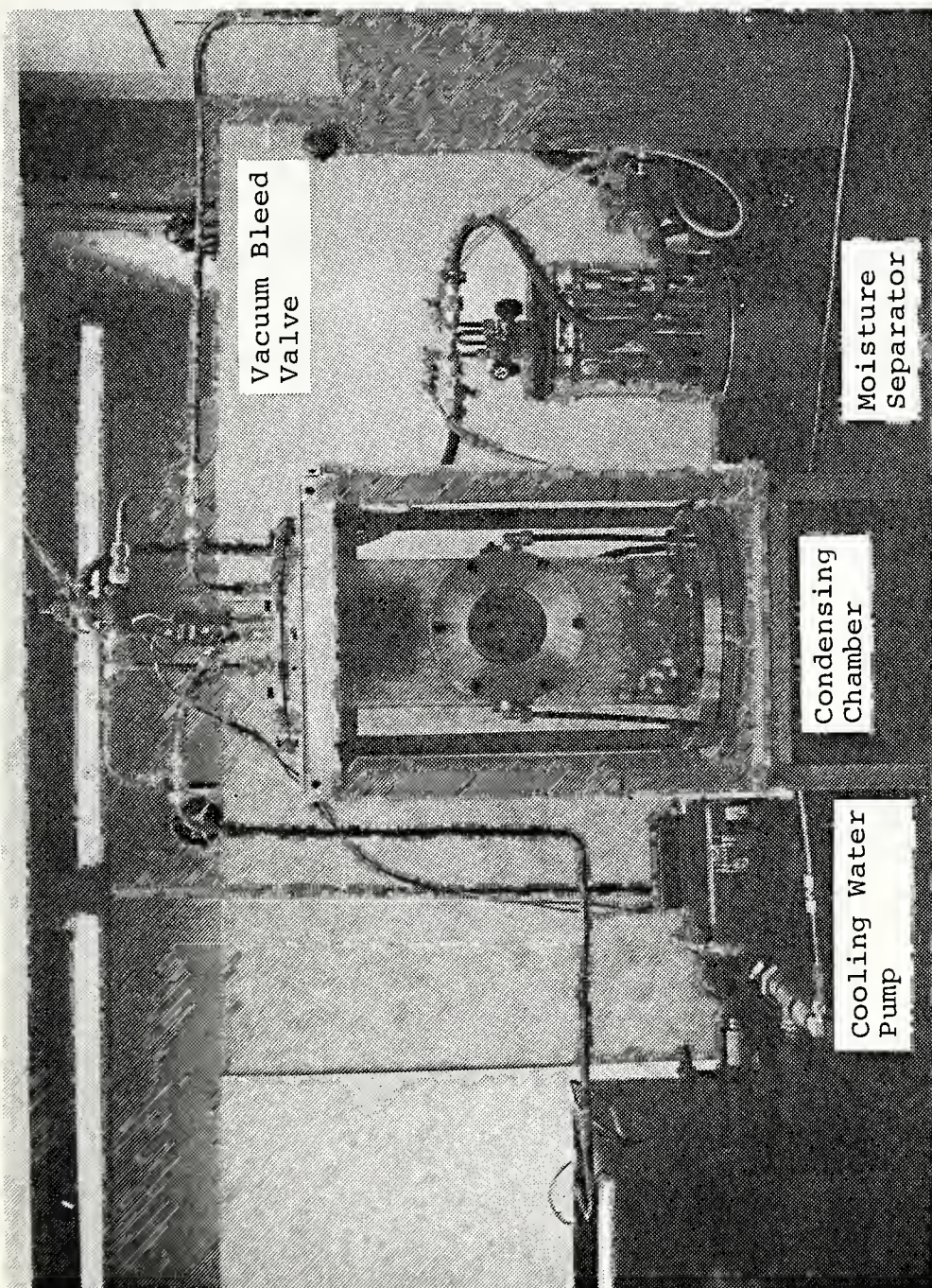


Figure 6 - Photograph of the Front of the Condensing Chamber

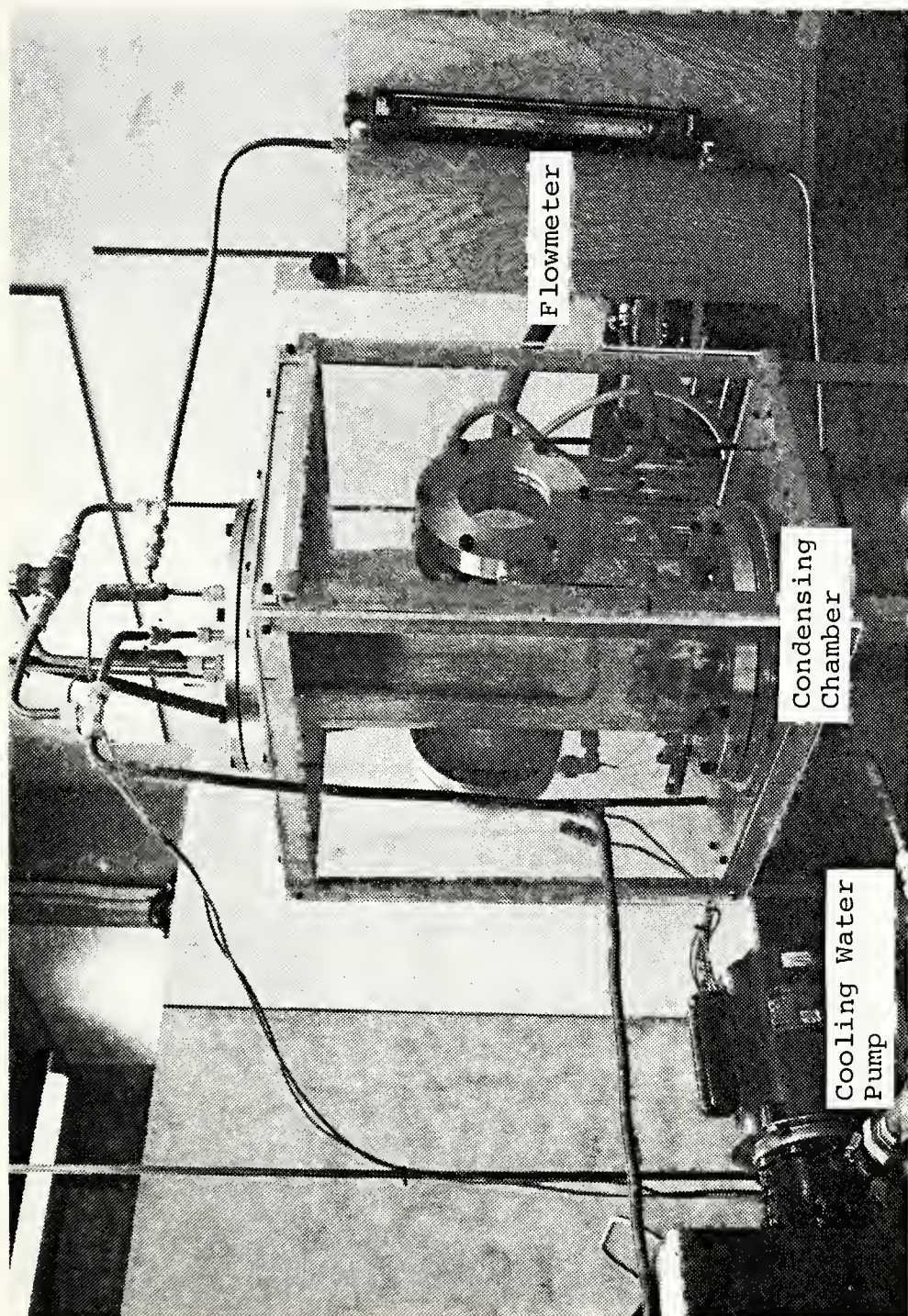


Figure 7 - Photograph of the Front, Left Side of the Condensing Chamber

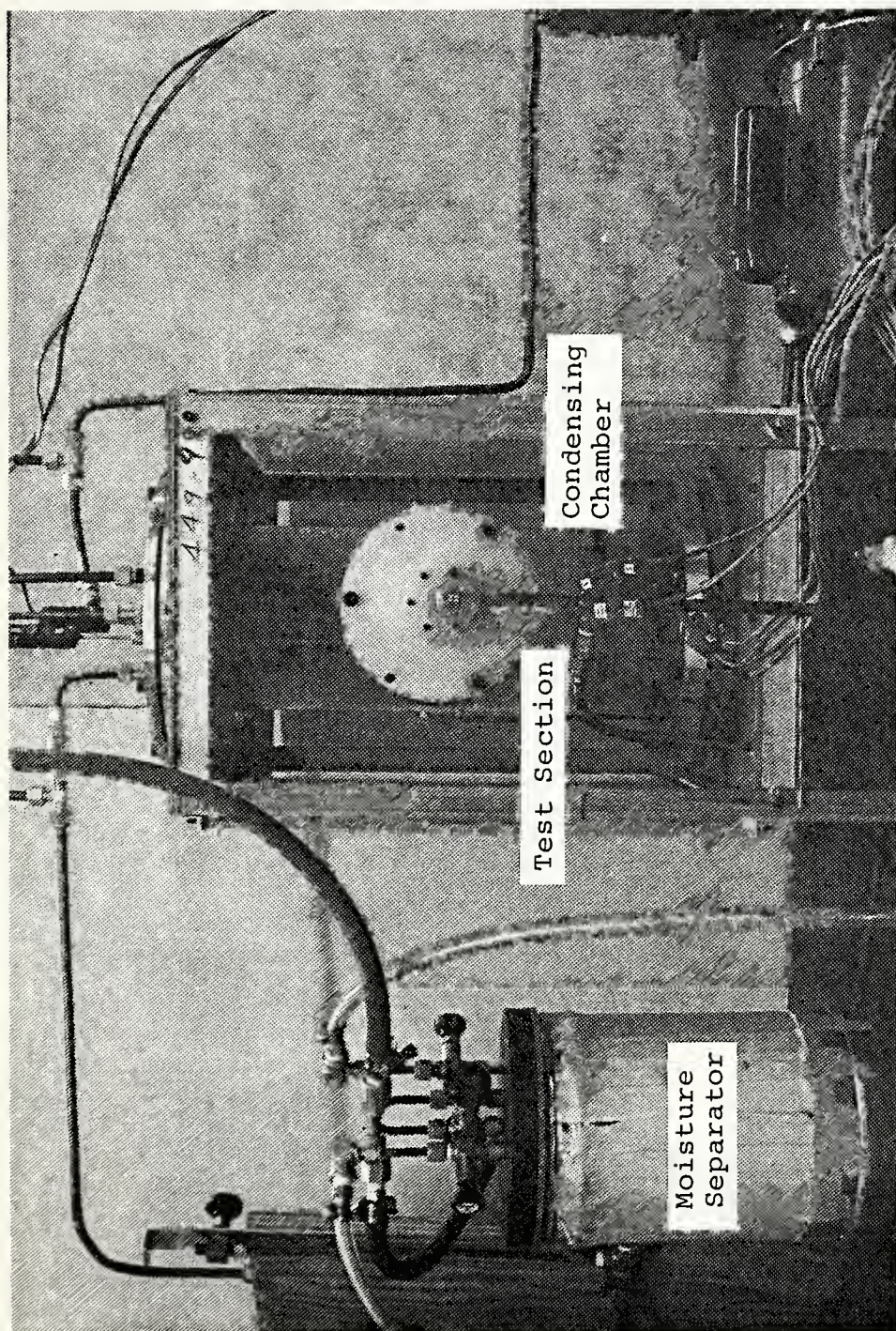


Figure 8 - Photograph of Rear of the Condensing Chamber

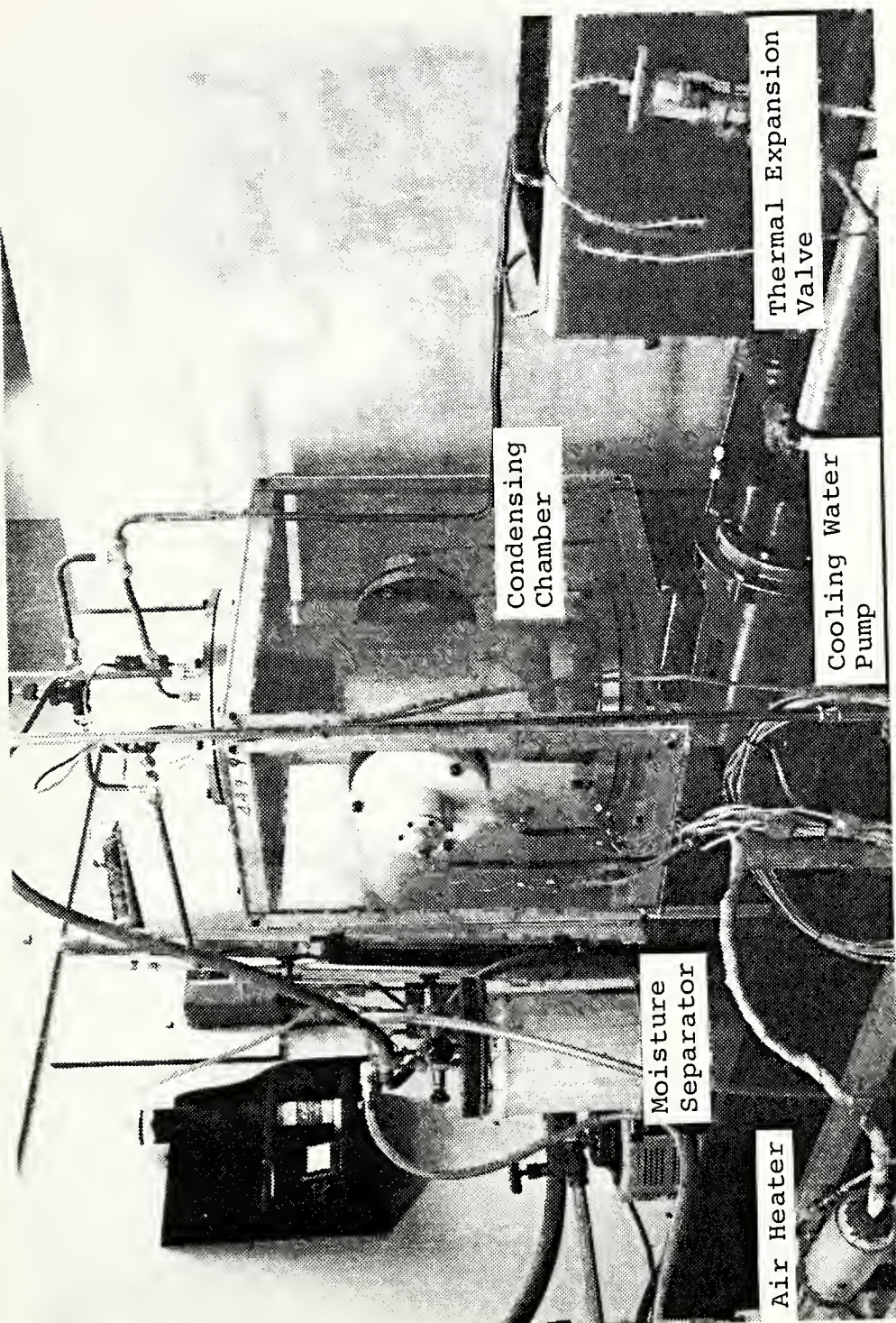


Figure 9 - Photograph of Rear, Left Side of the Condensing Chamber

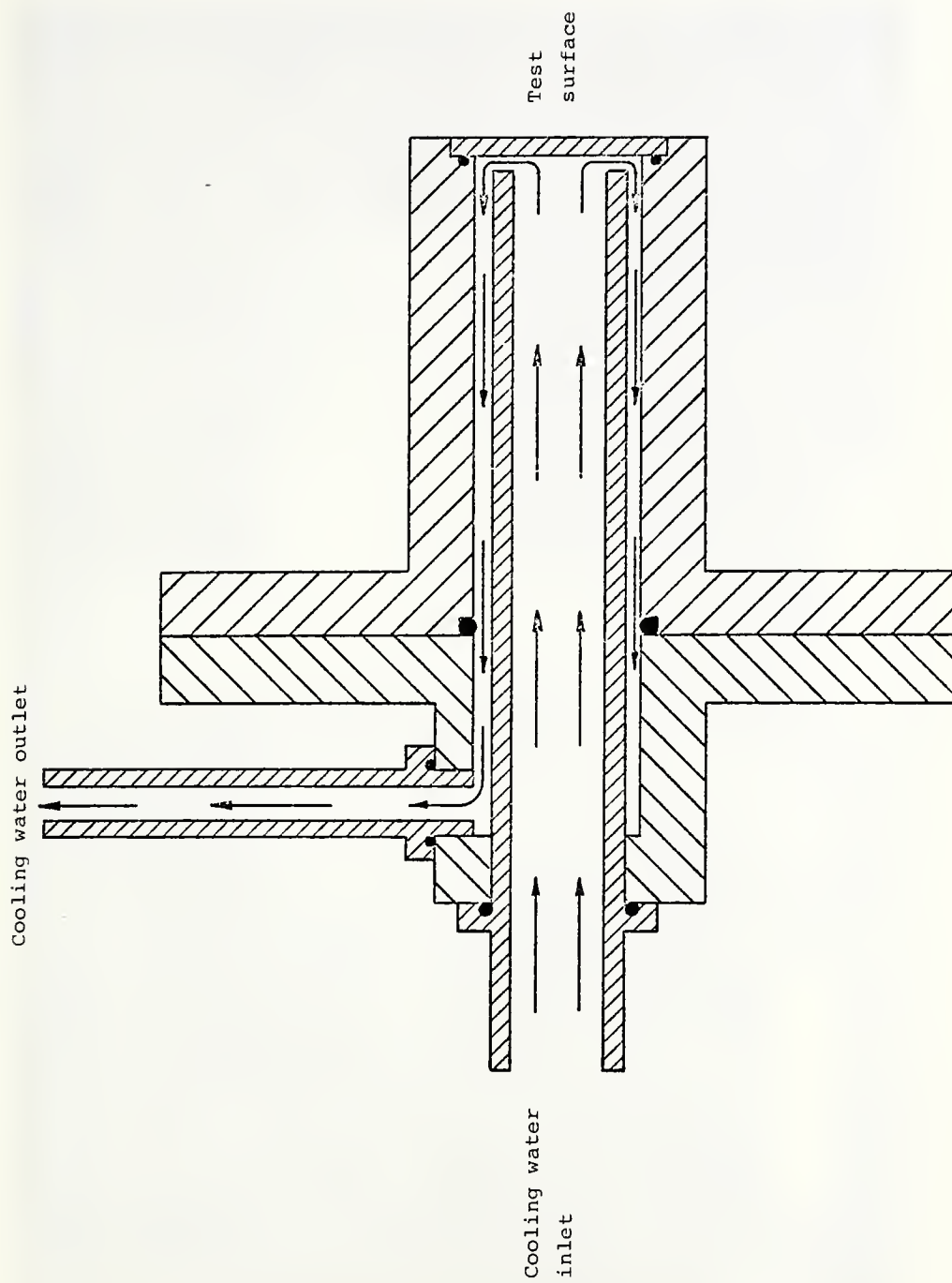


Figure 10 - Details of Condenser Test Section

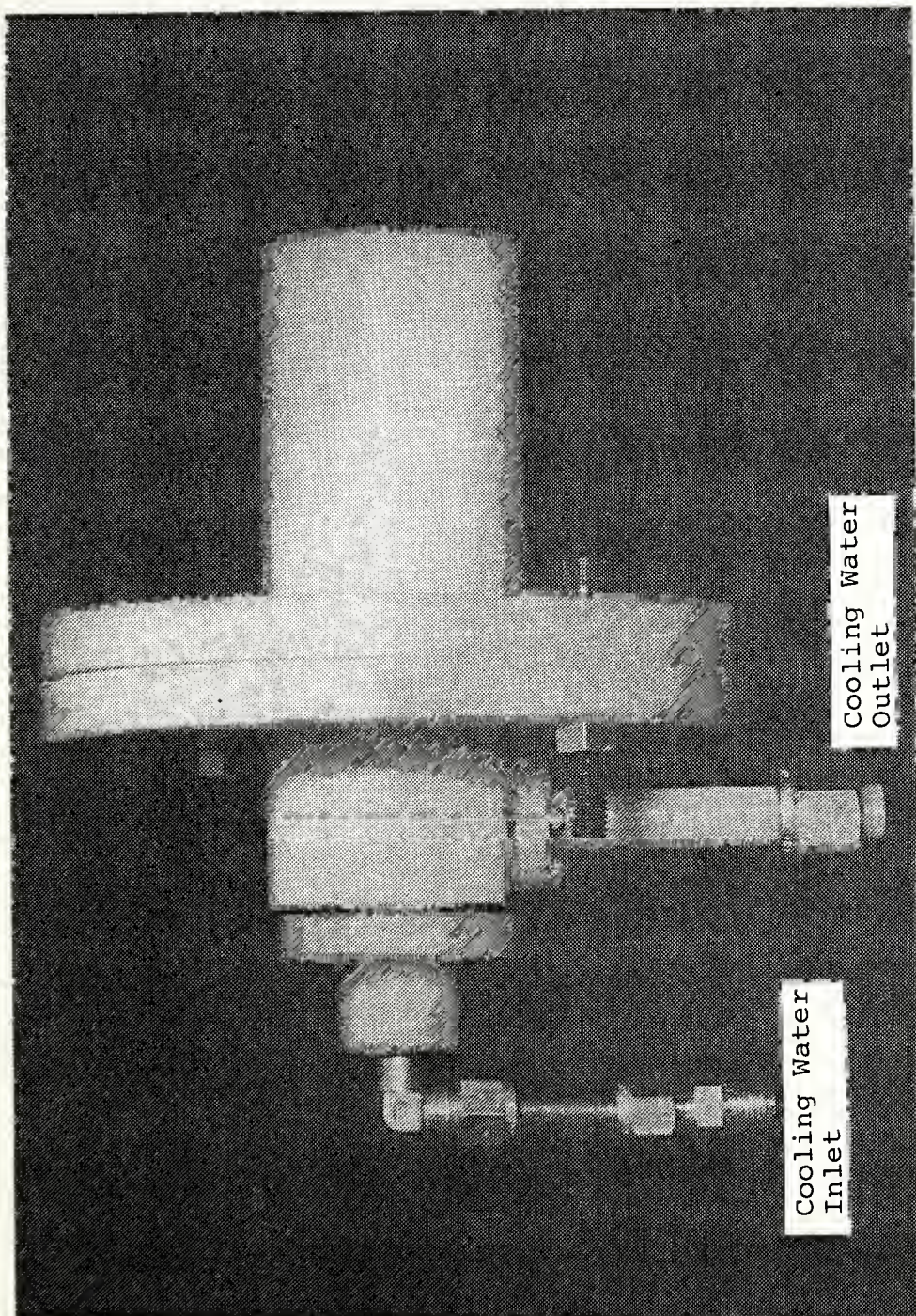


Figure 11 - Photograph of Condenser Test Section

Note: All dimensions are in millimeters.

Technical drawing showing a cross-section of a mechanical assembly. The drawing includes the following dimensions and features:

- Overall width: 152.4
- Top flange thickness: 12.7
- Central bore diameter: 38.1
- Shaft diameter: 28.58
- Inner bore diameter: 41.27
- Outer bore diameter: 57.15
- Flange thickness: 3.17
- Distance from top flange to inner bore: 82.55
- O-ring groove 1.59 (pointing to the top flange)
- O-ring groove 3.17 mm deep (pointing to the bottom flange)

Figure 12 - Details of Test Section Front Chamber

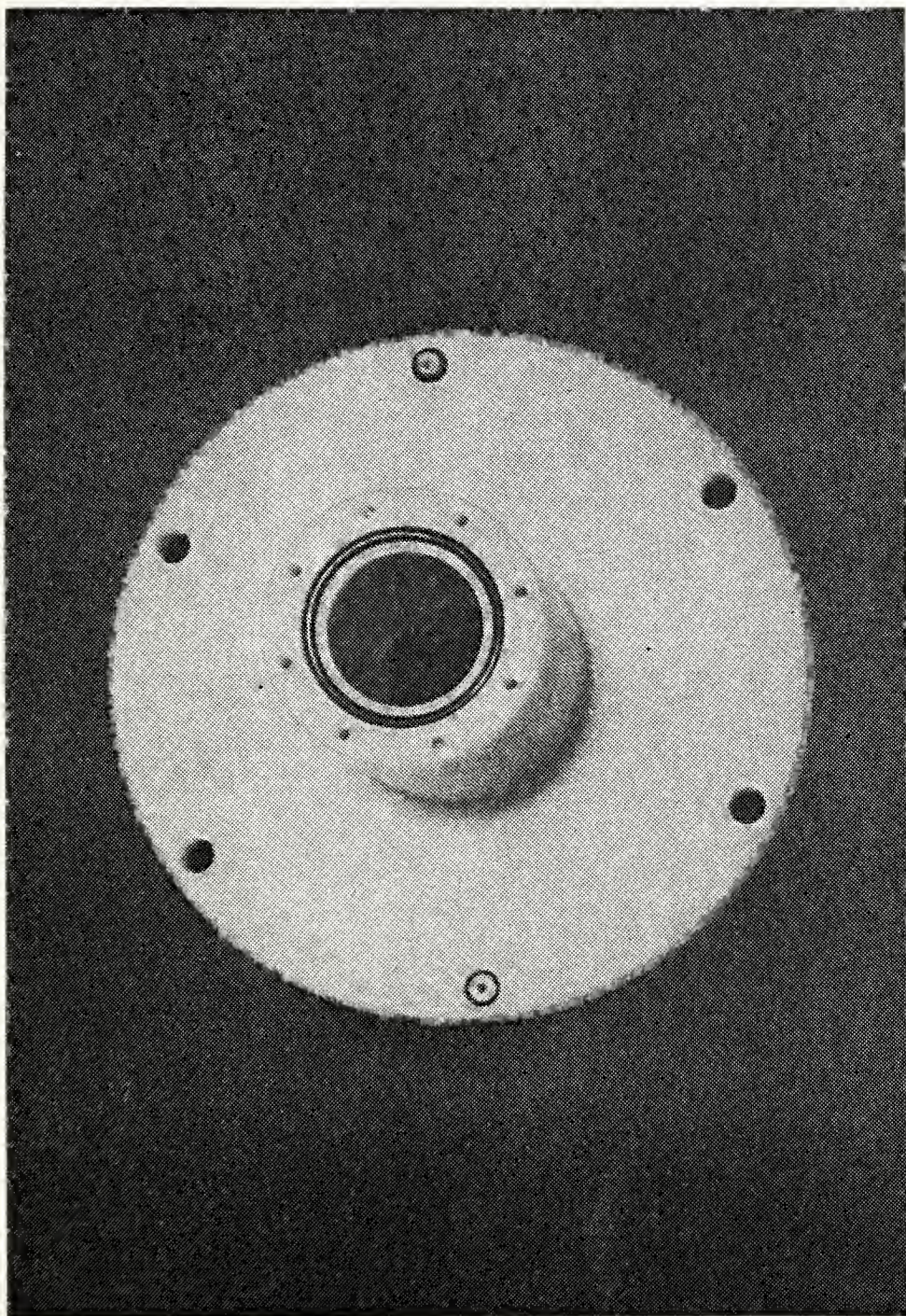


Figure 13 - Photograph of Test Section Front Chamber

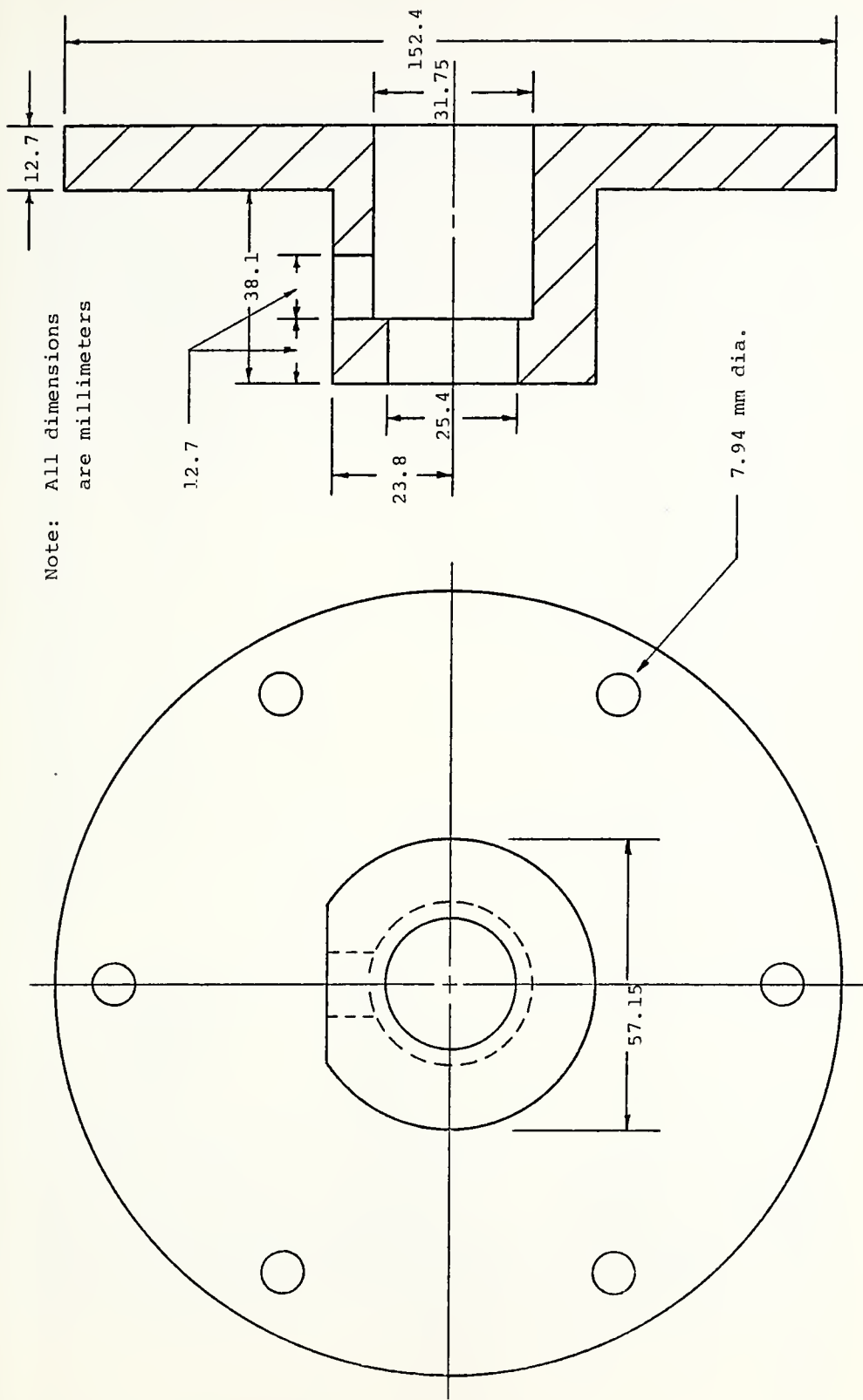
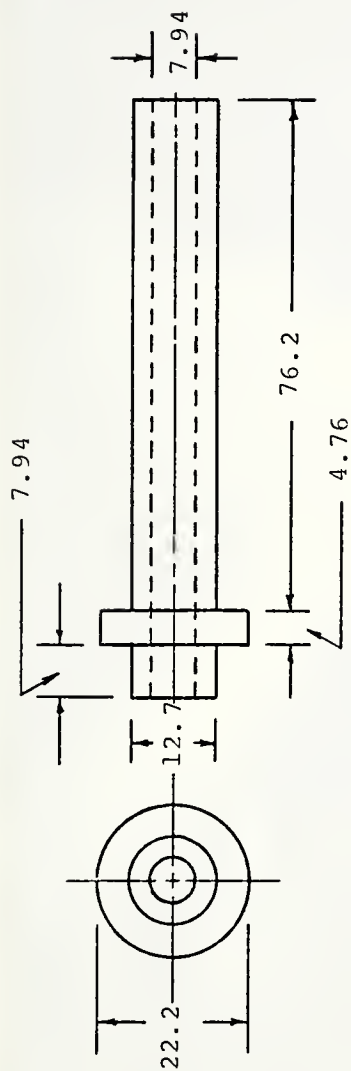


Figure 14 - Details of Test Section Rear Chamber



Note: All dimensions
are millimeters

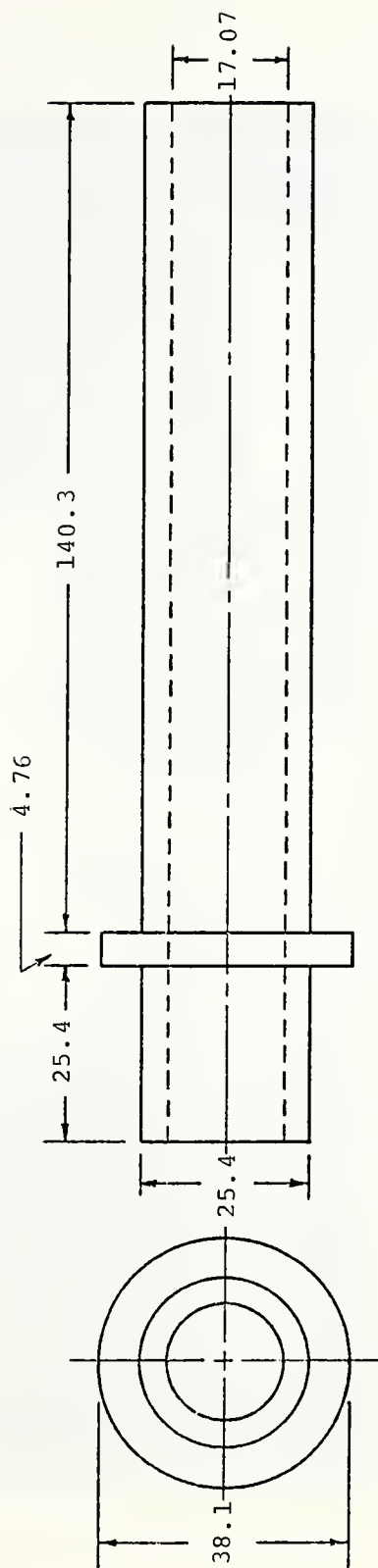


Figure 15 - Details of Cooling Water Inlet and Outlet Tubes

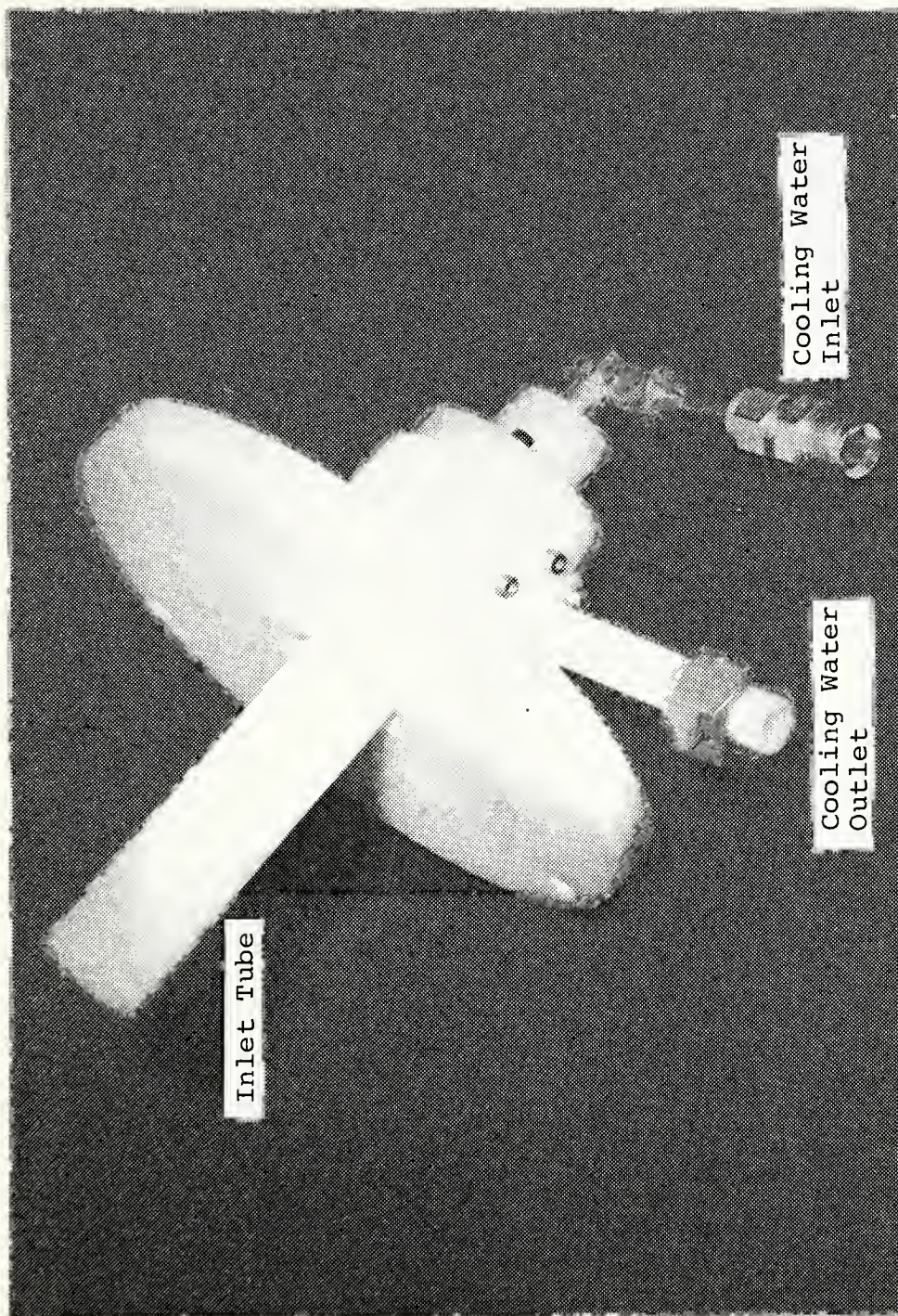


Figure 16 - Side View of Test Section Rear Chamber With Inlet and Outlet Tubes Installed

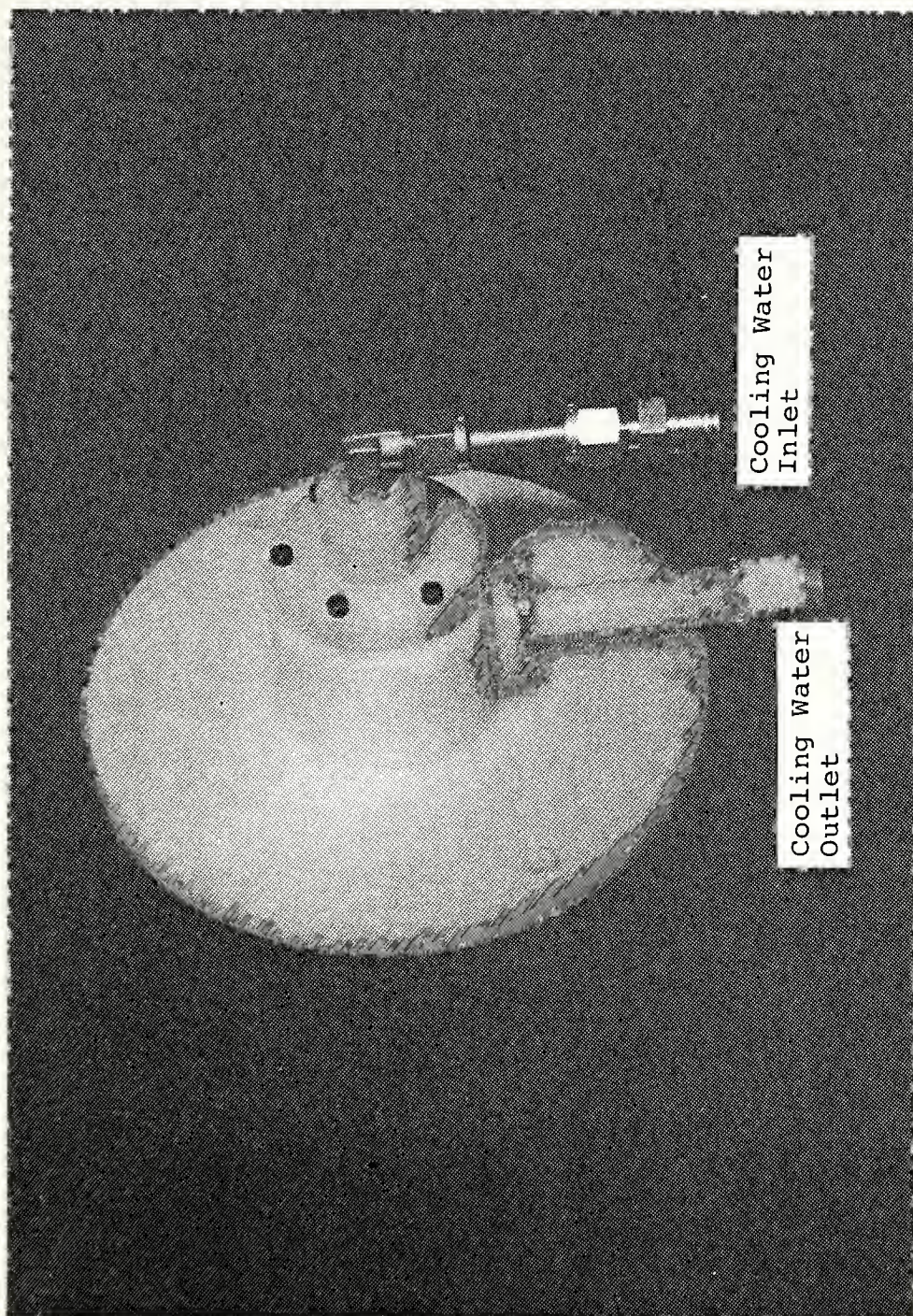


Figure 17 - Rear View of Test Section Rear Chamber With Inlet and Outlet Tubes Installed

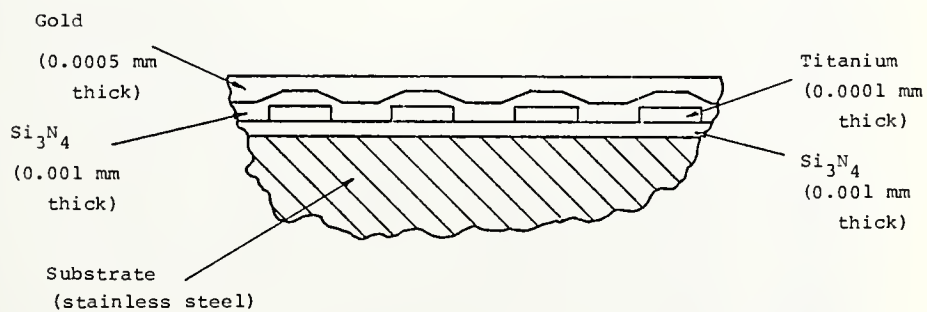
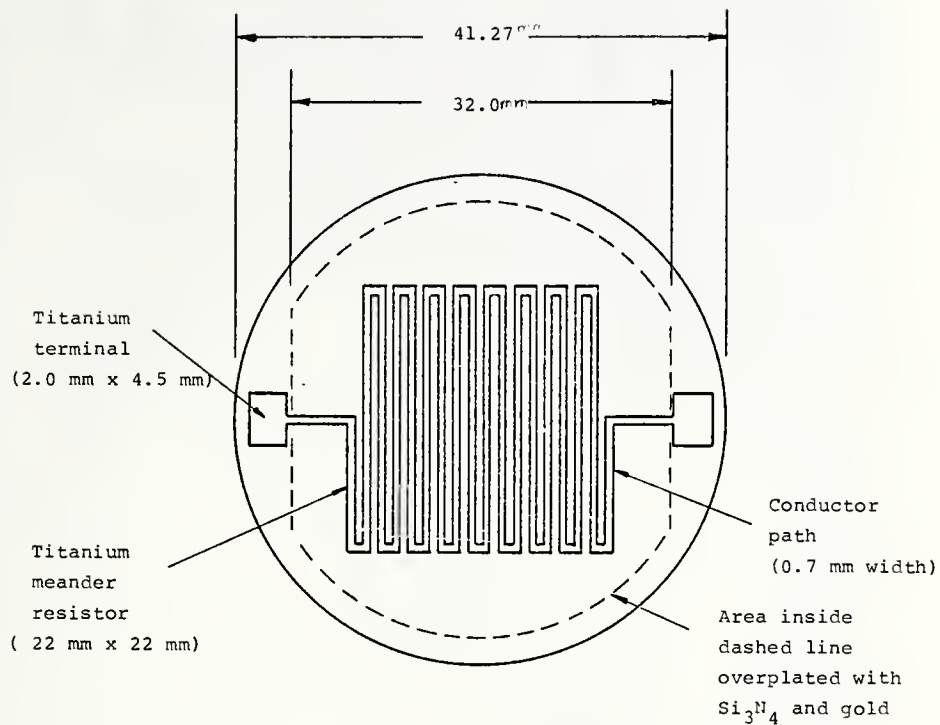


Figure 18 - Details of Test Surface

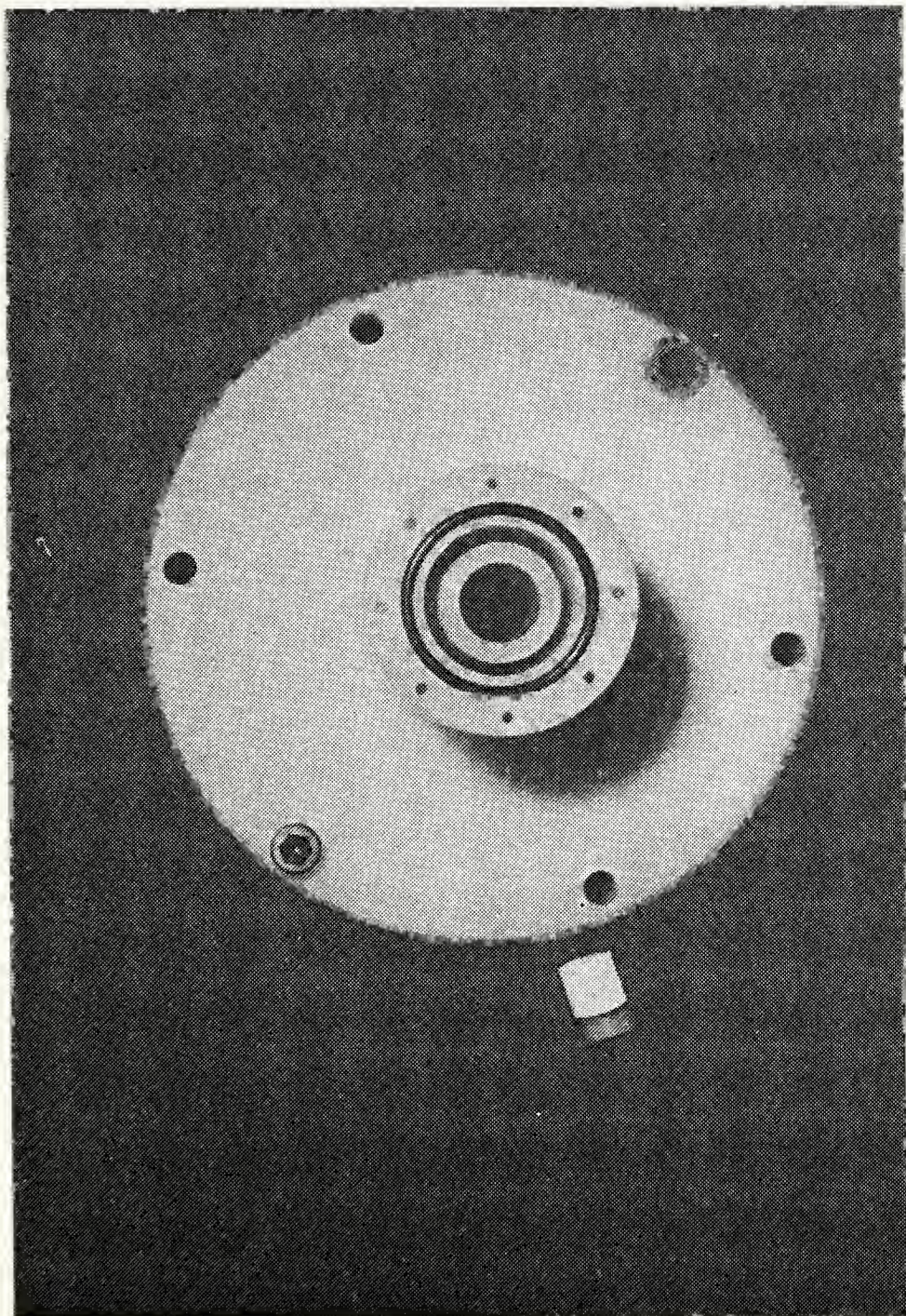


Figure 19 - Photograph of "O"-Ring Seal on Front Chamber Face

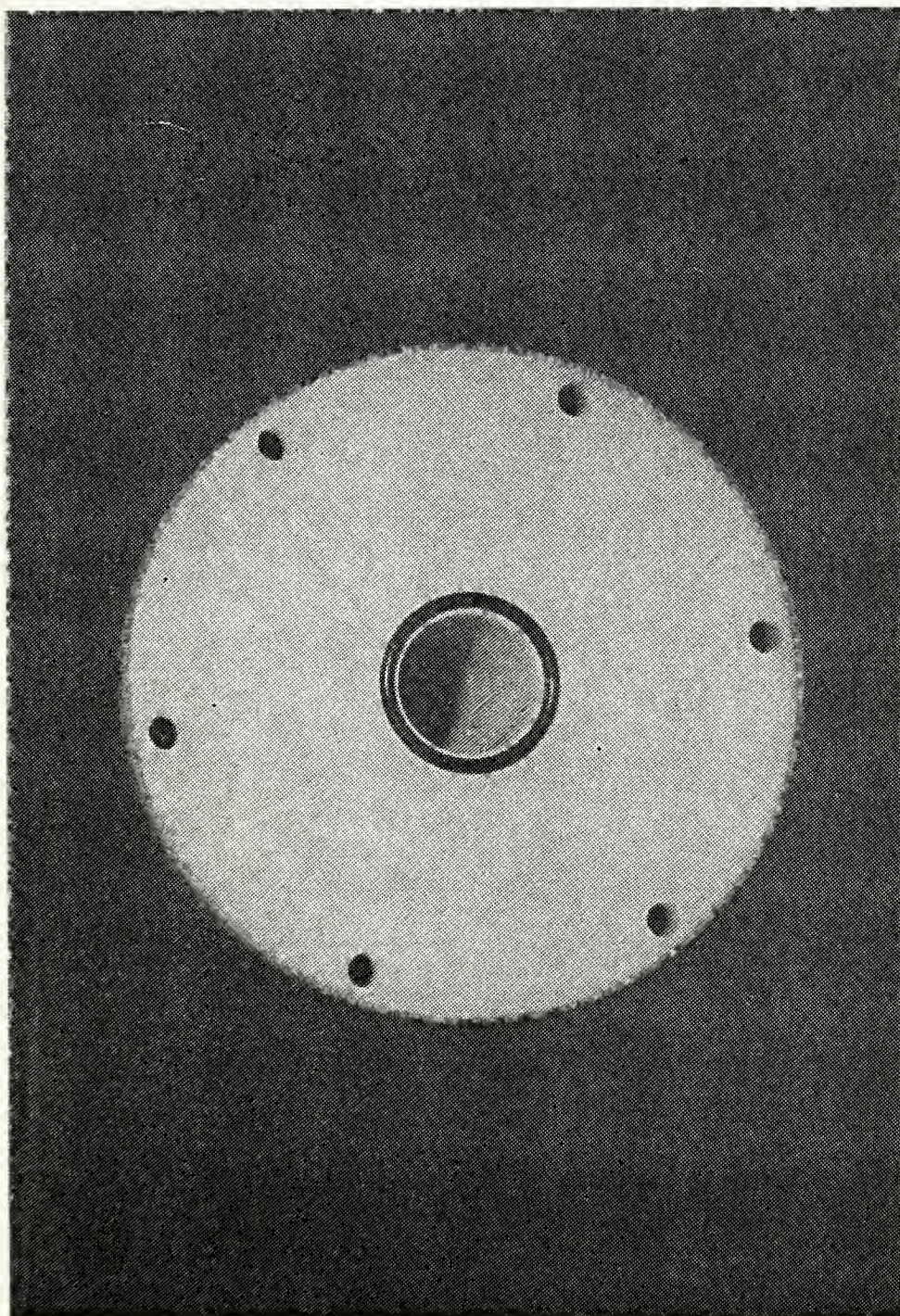


Figure 20 - Photograph of "O"-ring Seal on Back of Front Chamber

Note: All dimensions
are millimeters

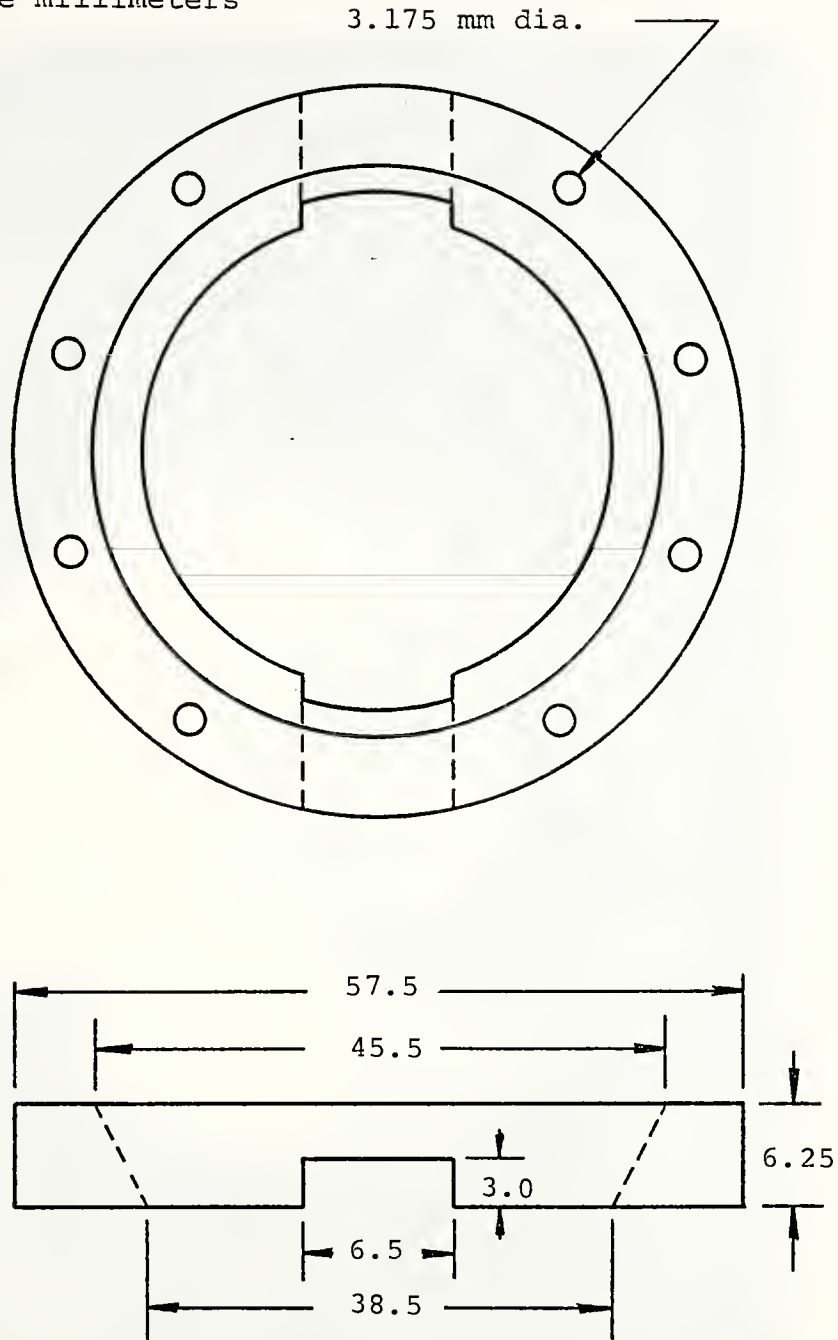


Figure 21 - Details of Test Surface Retaining Ring

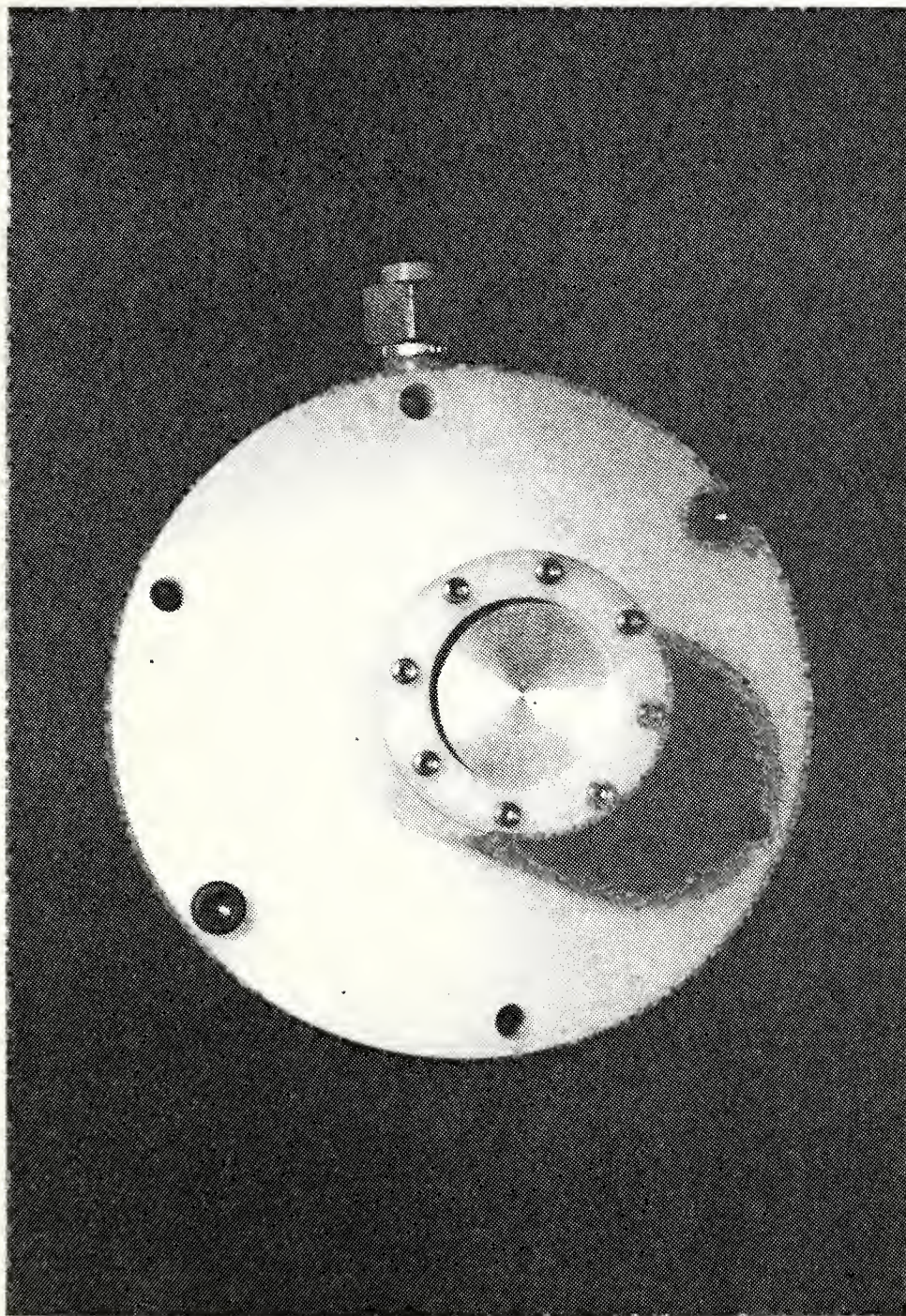


Figure 22 - Photograph of Retaining Ring and Test Surface on Front Chamber Face

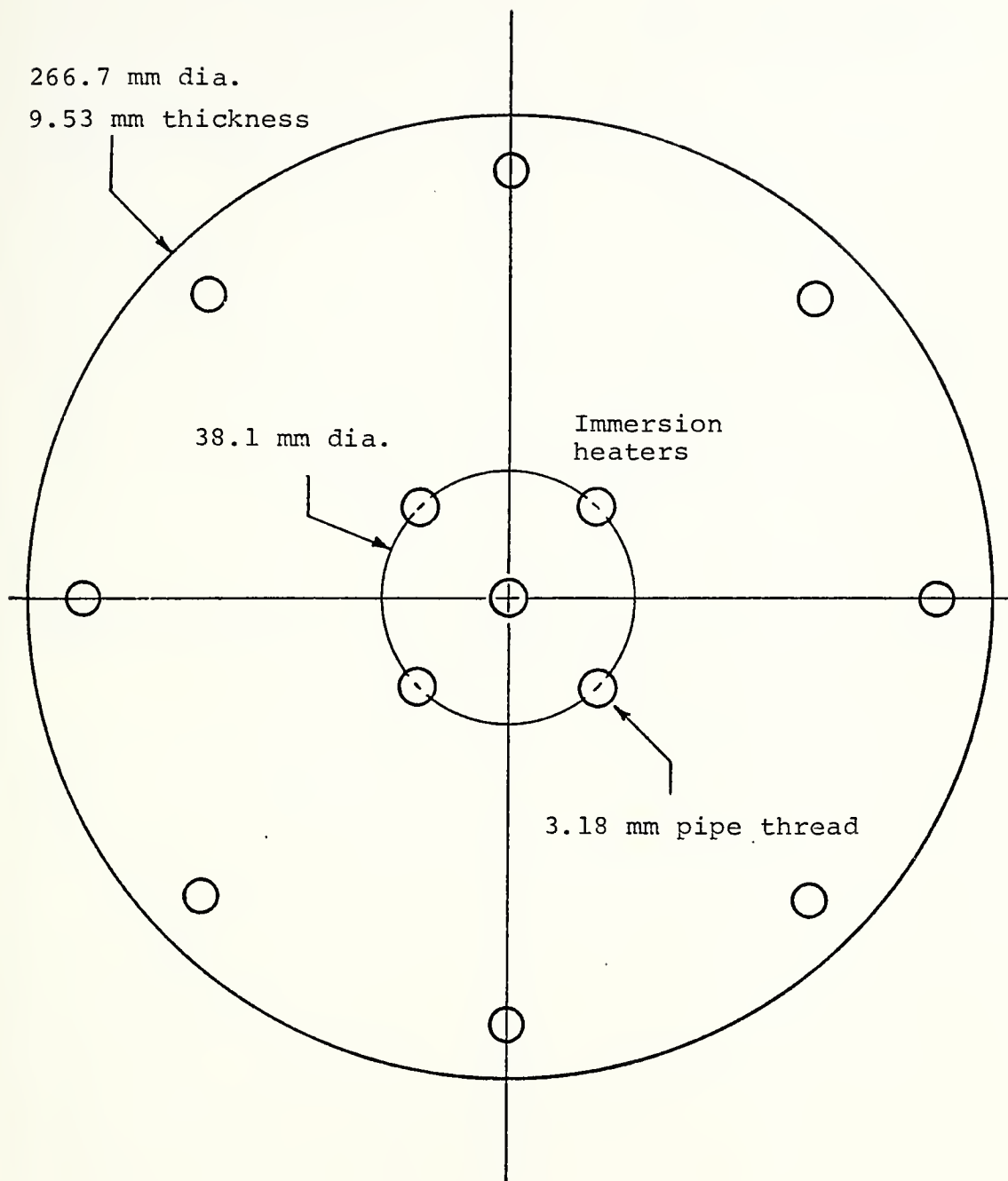


Figure 23 - Details of Bottom End Plate

Note: All dimensions
are millimeters

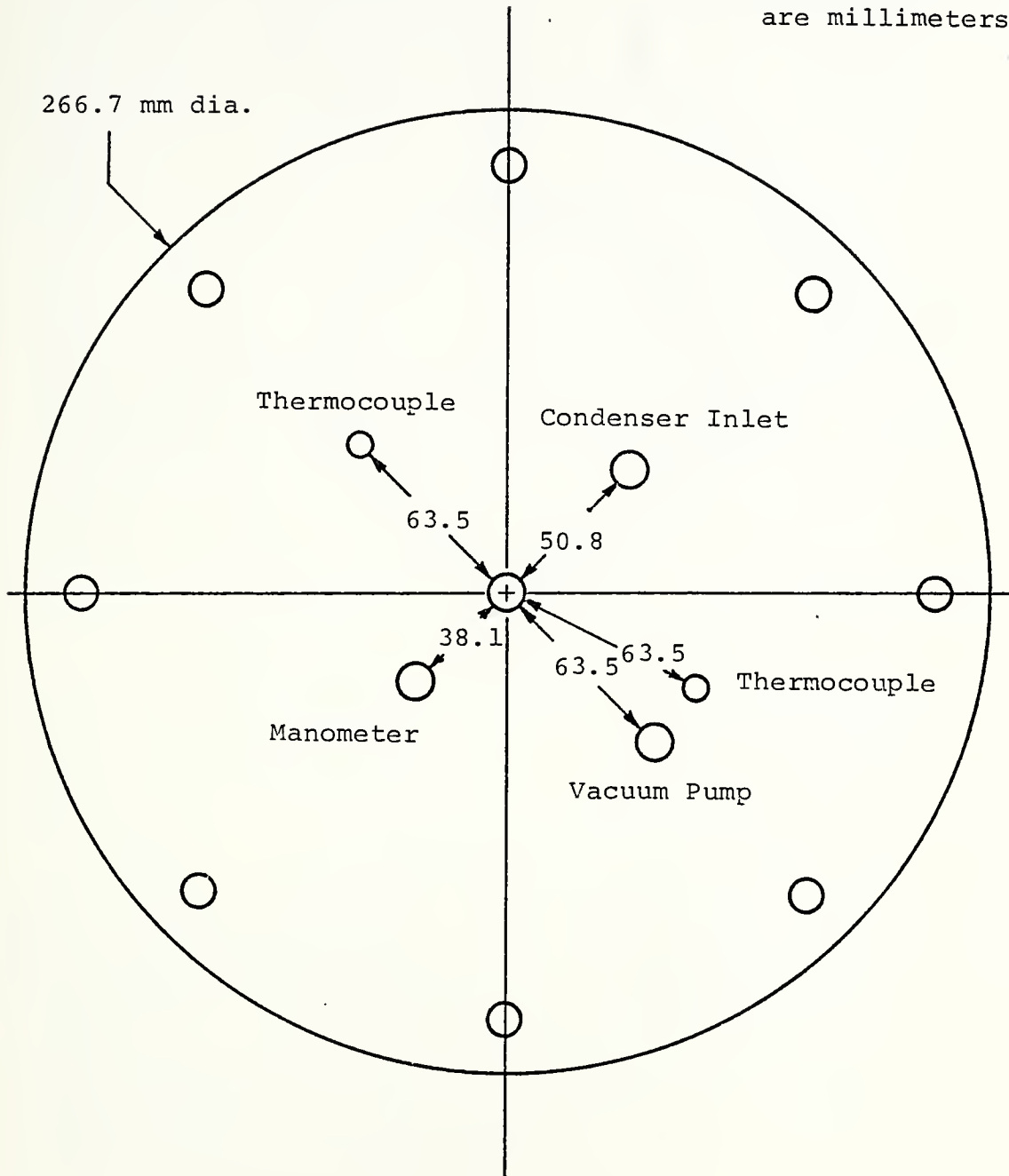


Figure 24 - Details of Top End Plate

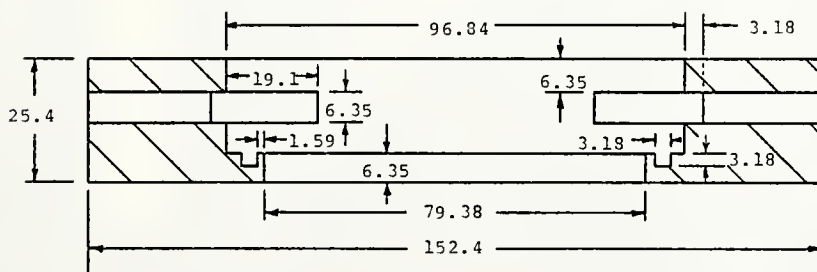
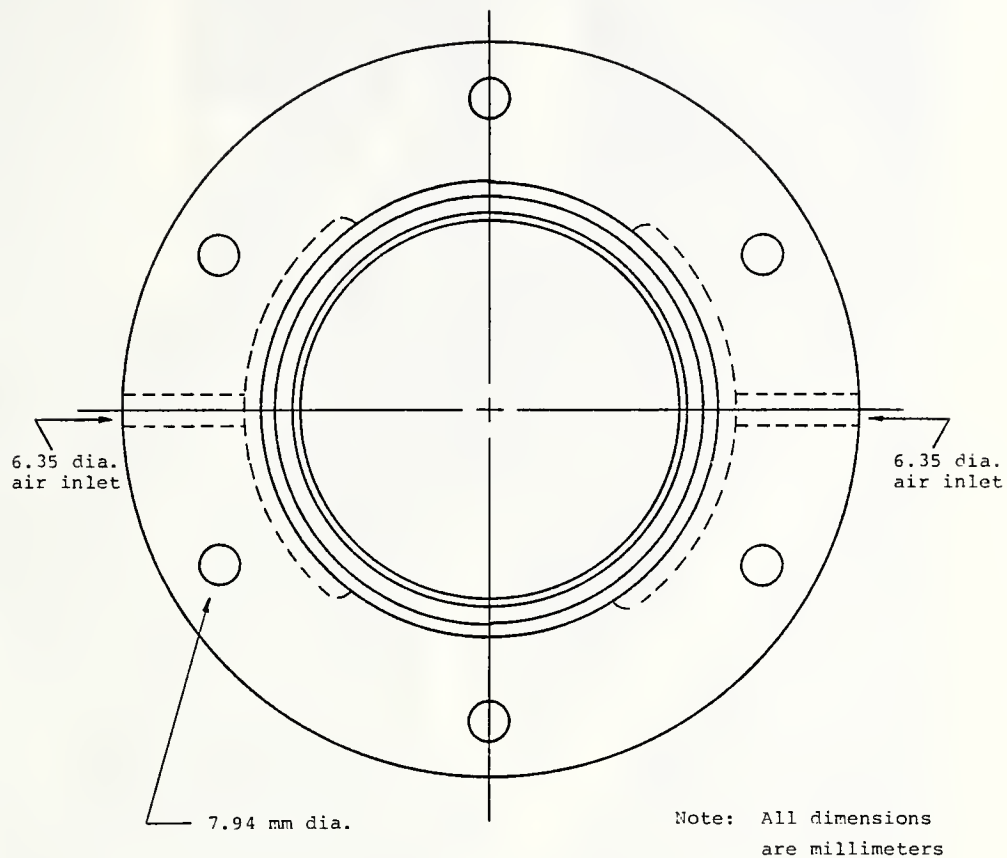


Figure 25 - Details of Observation Port Support Frame

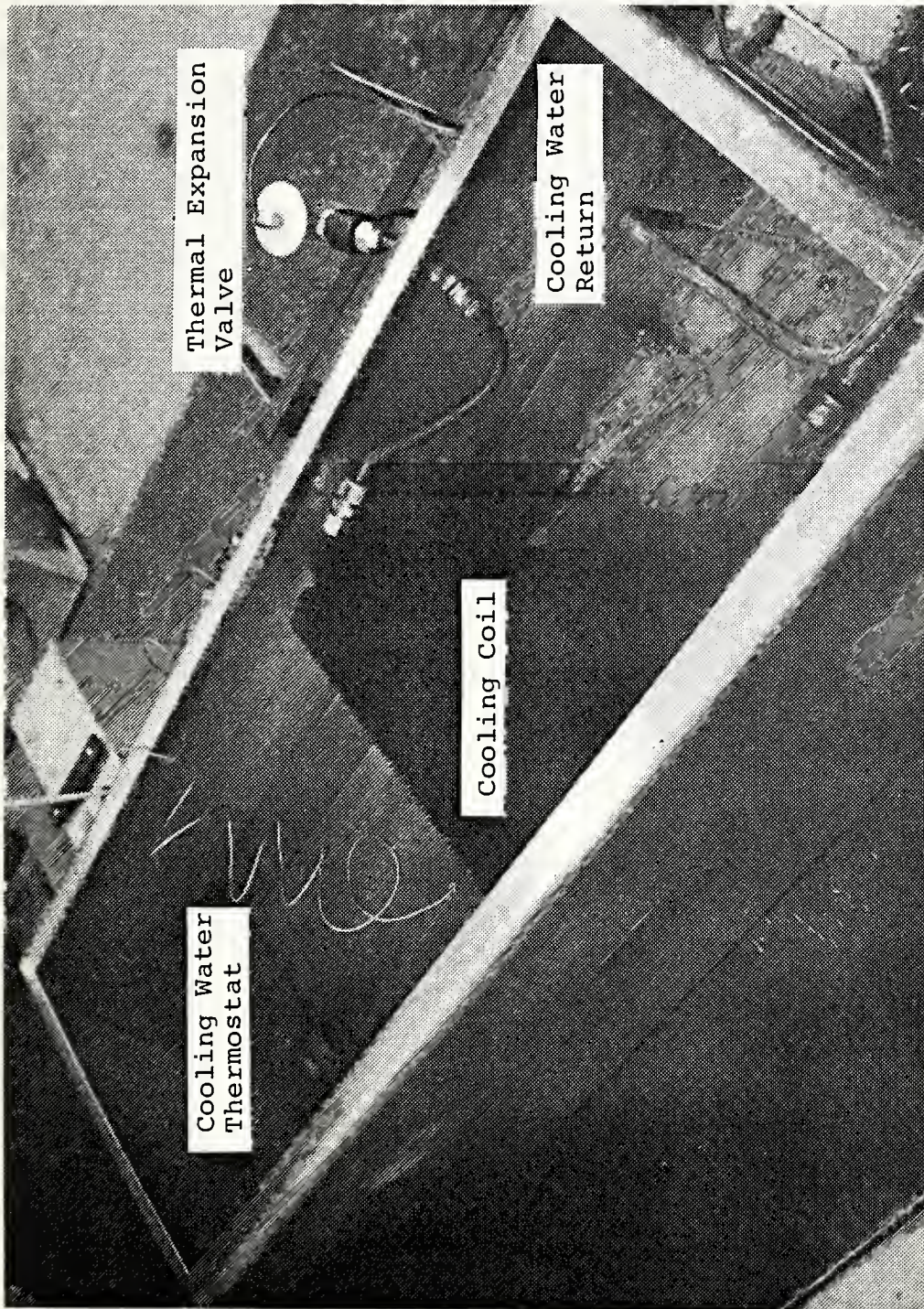


Figure 26 - Photograph of Storage Reservoir

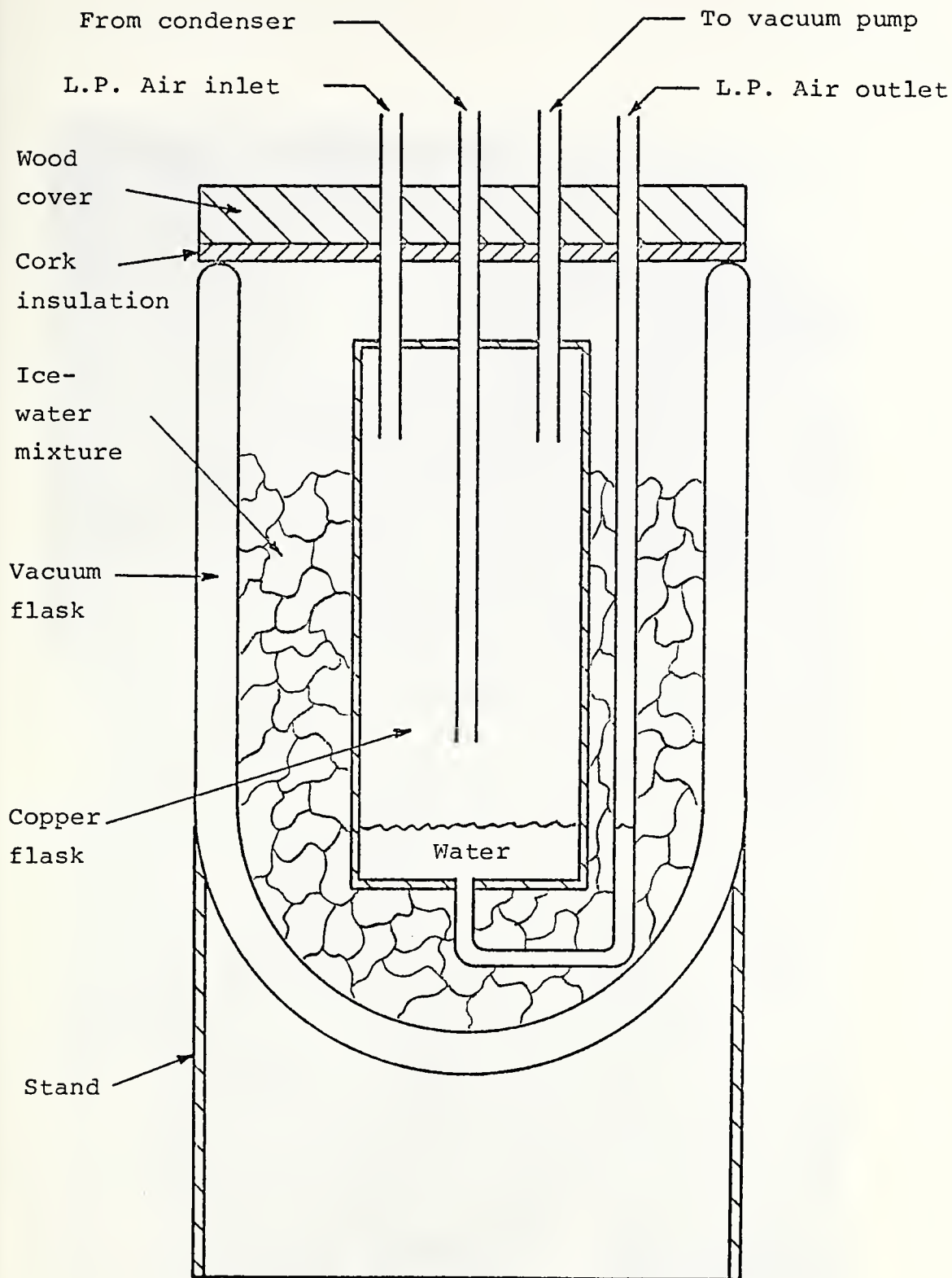


Figure 27 - Details of Moisture Separator

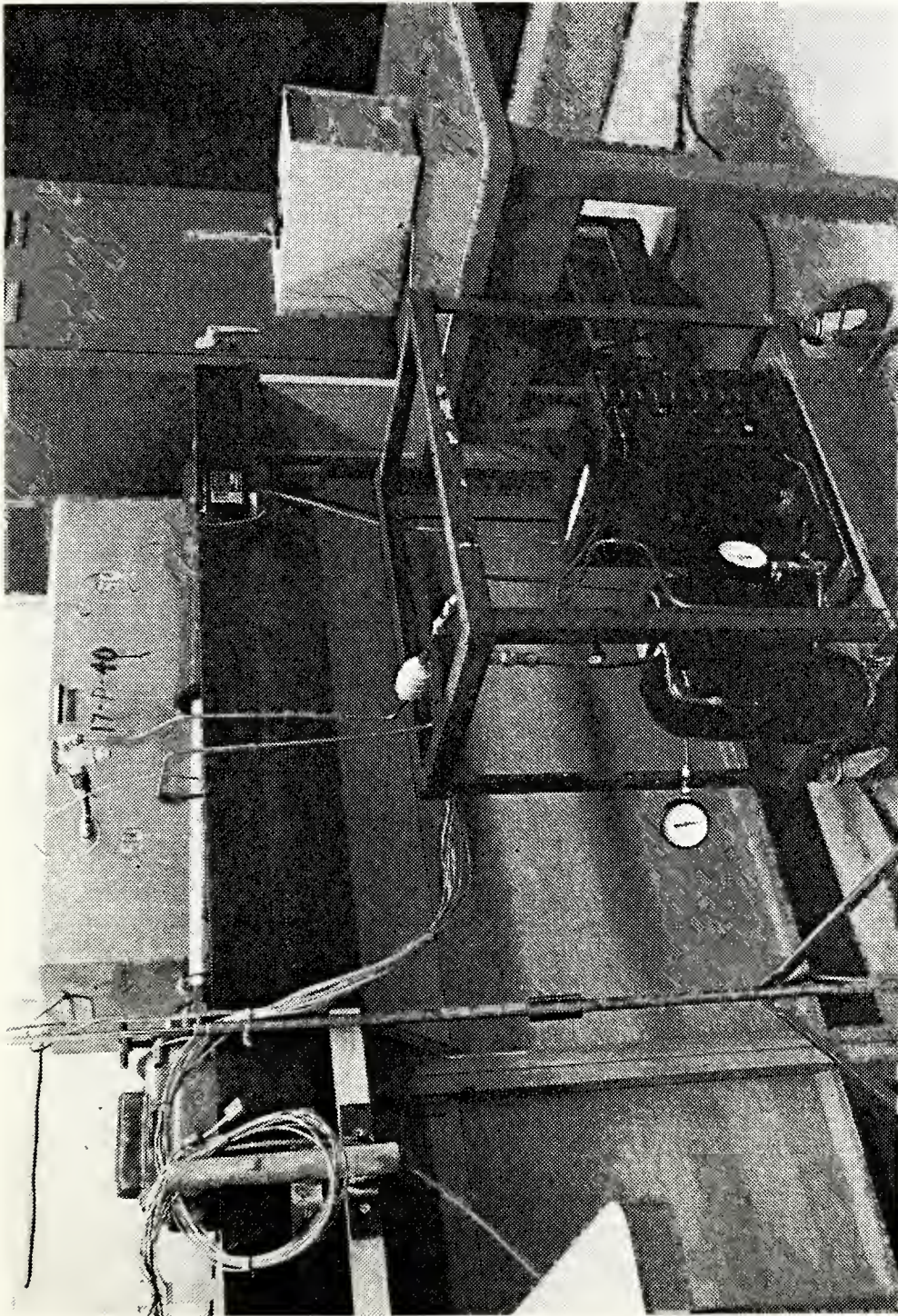


Figure 28 - Photograph of Refrigeration System

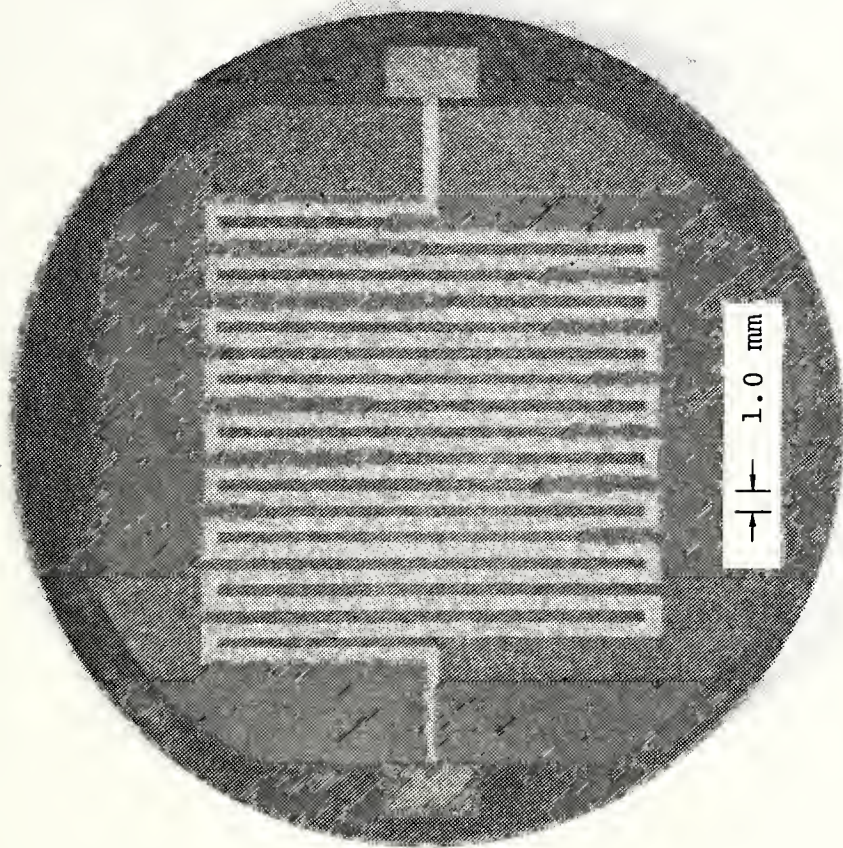


Figure 29 - Photograph of Test Surface Showing Etched Titanium Meander Thermometer

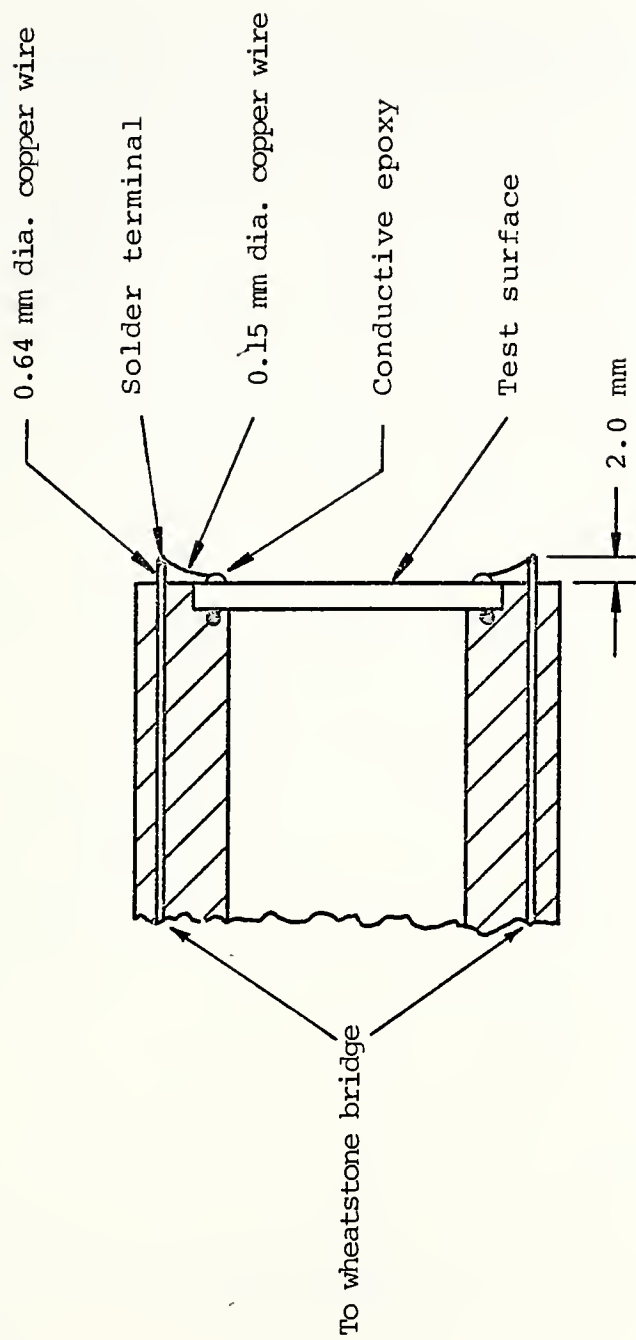


Figure 30 - Details of Test Surface Installation In Condenser Test Section

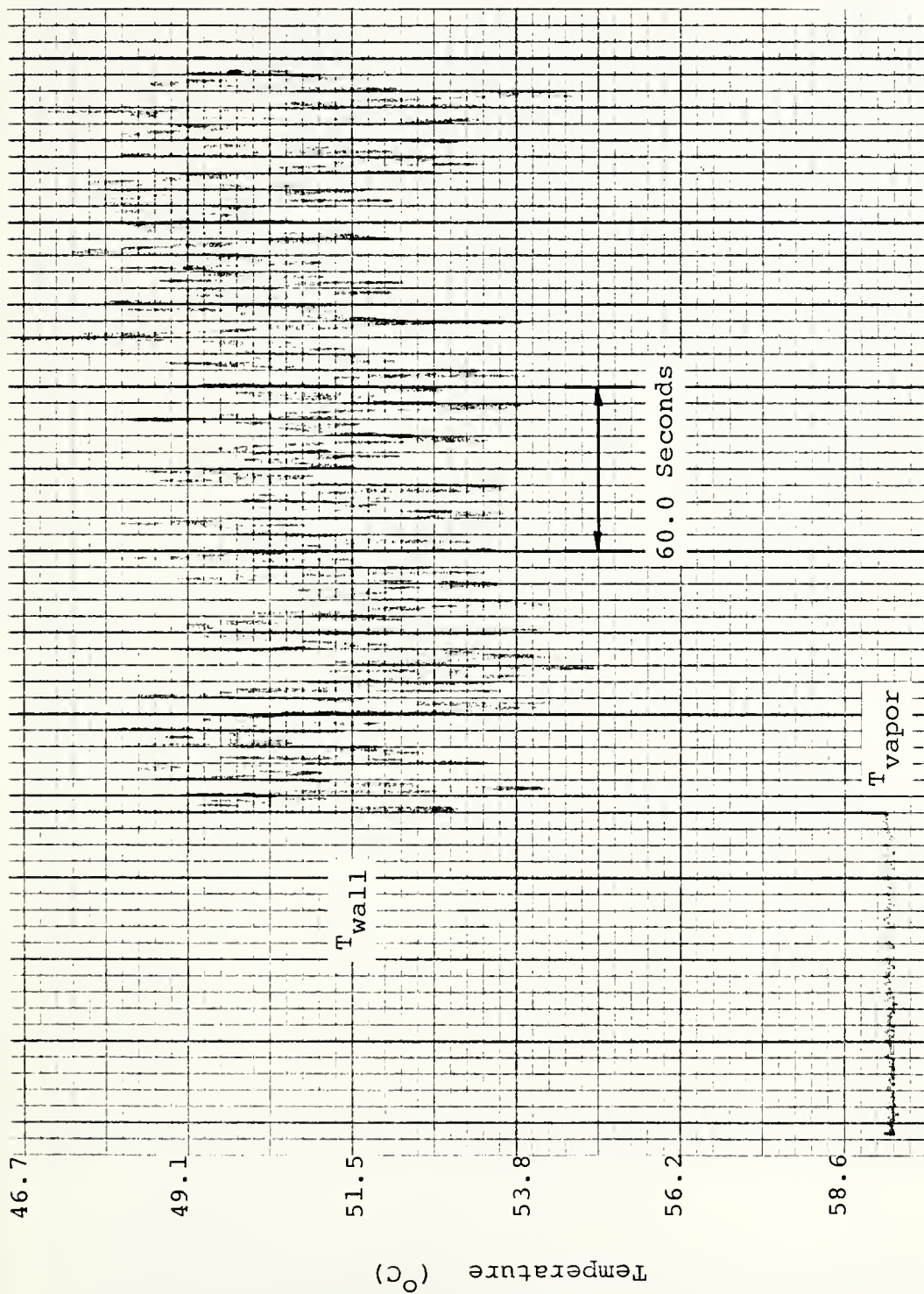


Figure 31 - Temperature Fluctuation on the Condensing Surface Recorded
By the Intrinsic Thermocouple at a ΔT of 6.97 °C

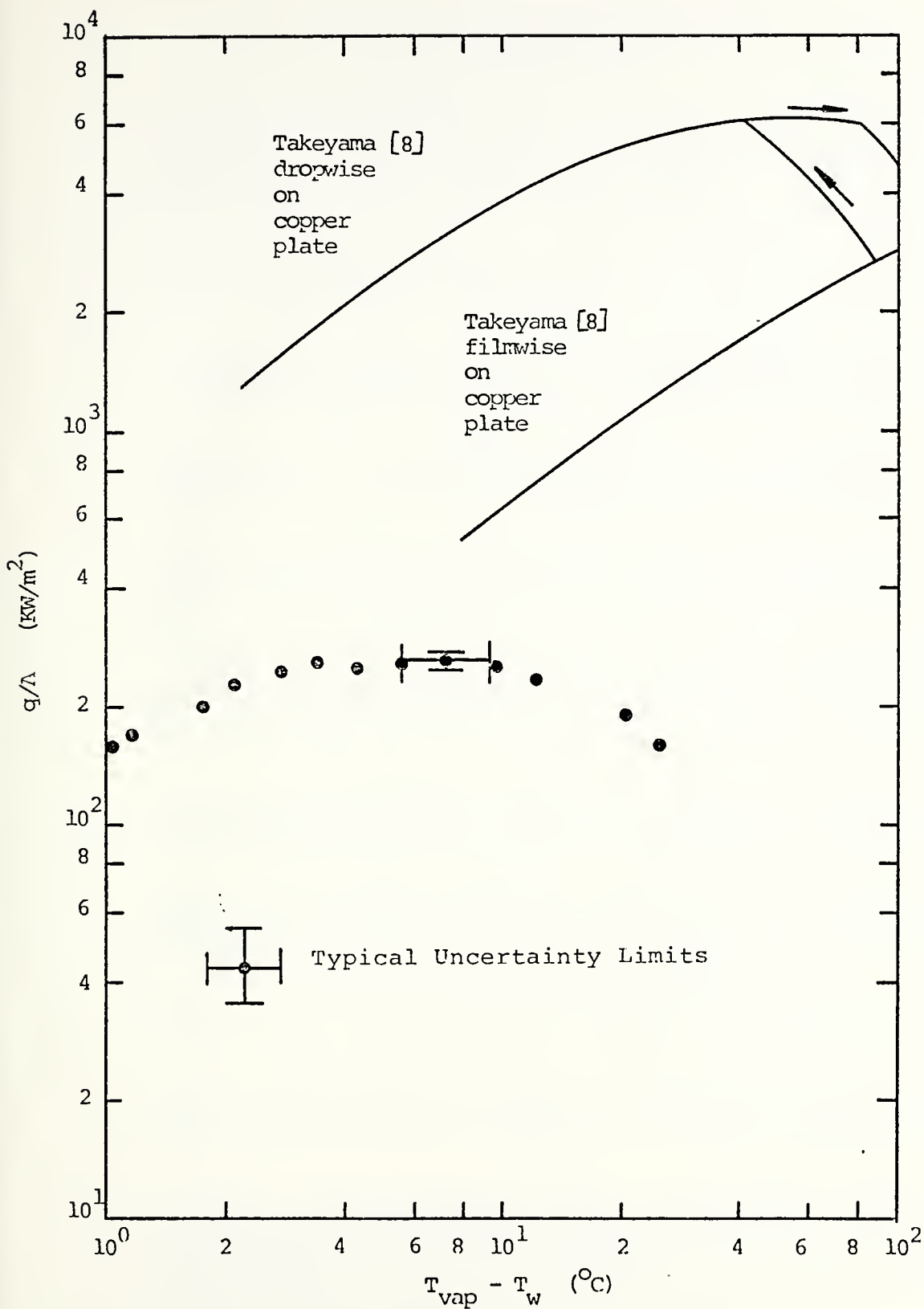


Figure 32 - Comparison of Experimental Data With The Condensing Curve Proposed by Takeyama[8]

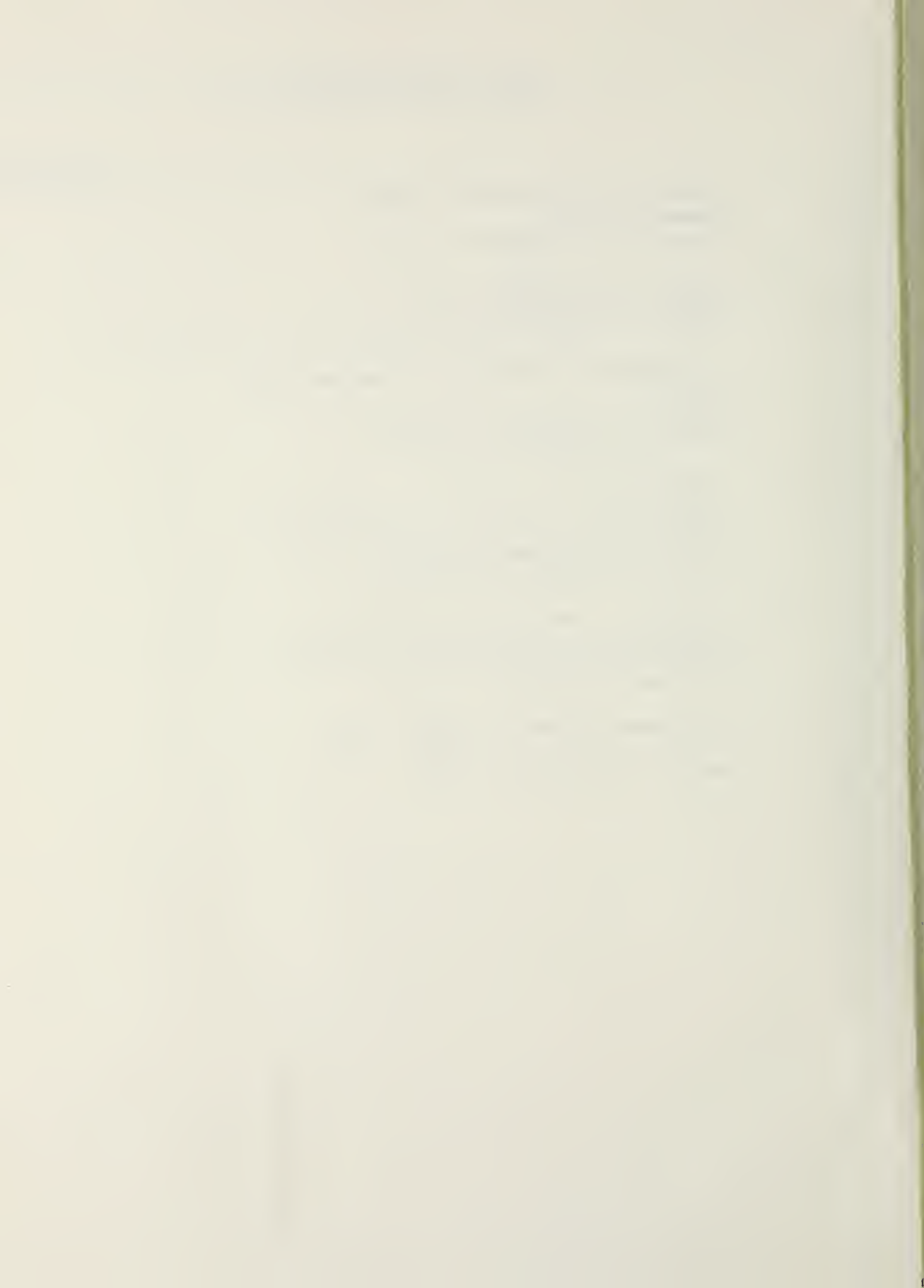
LIST OF REFERENCES

1. Schmidt, E., W. Shuring, and W. Sellschopp, "Versuche Uber die Kondensation von Wasserdampf in Film-und Tropfenform," Tech. Mech. Thermo-Dynam, v. 1, p. 53, 1930.
2. Jakob, M., "Heat Transfer in Evaporation and Condensation-II," Mechanical Engineering, v. 58, p. 729-739, 1936.
3. Tammann, G., and W. Boehme, "Die Zahl der Wassertropfen bei der Kondensation auf verschiedenen festen stoffen," Annalen der Physik, v. 5, p. 77-80, 1935.
4. Umur, A., and P. Griffith, "Mechanism of Dropwise Condensation," ASME, Paper 64-WA/HT-3, Journal of Heat Transfer, p. 275-282, 1965.
5. Graham, C., and W.F. Aerni, "Dropwise Condensation: A Heat Transfer Process for the '70s," Naval Ship System Command Tech. News, v. 19, p. 8-15, July, 1970.
6. Magrini, U., and E. Nannei, "On the Influence of the Thickness and Thermal Properties of Heating Walls on the Heat Transfer Coefficients in Nucleate Pool Boiling," ASME Paper 75-HT-TT, Journal of Heat Transfer, v. 97, p. 173-178, 1975.
7. Chuck, T.L., and Myers, J.E., "The Effect of Heater Plate Thickness on Boiling Heat Transfer Coefficients," Int. J. Heat Mass Transfer, v. 21, p. 187-191, 1978.
8. Takeyama, T., and S. Shimizu, "On the Transition of Dropwise-Film Condensation," International Heat Transfer Conference, 5th Proceedings, Tokyo, Japan, September 3-7, 1974, v. 3, Paper Cs 2.5, p. 274-278.
9. Mikic, B.B., "On Mechanism of Dropwise Condensation," Int. J. Heat Mass Transfer, v. 12, p. 1311-1323, 1969.
10. Hurst, C.J., and D.R. Olson, "Conduction Through Drop-lets during Dropwise Condensation," ASME, Paper 72-HT-50, 1972.
11. Hannemann, R.J., and B.B. Mikic, "An Analysis of the Effect of Surface Thermal Conductivity on the Rate of Heat Transfer in Dropwise Condensation," Int. J. Heat Mass Transfer, v. 19, p. 1299-1307, 1976.
12. Hannemann, R.J., and B.B. Mikic, "An Experimental Investigation into the Effect of Surface Thermal Conductivity on the Rate of Heat Transfer in Dropwise Condensation," Int. J. Heat Mass Transfer, v. 19, p. 1309-1317, 1976.

13. Hannemann, R.J., "Condensing Surface Thickness Effects in Dropwise Condensation," Int. J. Heat Mass Transfer, v. 21, p. 65-66, 1978.
14. Morgan, L.M., Some Experimental Observations of Dropwise Condensation of Steam, M.S.M.E. Thesis, Naval Postgraduate School, Monterey, California, 1972.
15. Metals Handbook, 8th ed., v. 2, p. 141, American Society for Metals, 1964.
16. Kline, S.J., and F.A. McClintock, "Describing Uncertainties in Single-Sample Experiments," Mechanical Engineering, v. 75, p. 3-8, January, 1953.

INITIAL DISTRIBUTION LIST

	<u>No. Copies</u>
1. Defense Documentation Center Cameron Station Alexandria, Virginia 22314	2
2. Library, Code 0142 Naval Postgraduate School Monterey, California 93940	2
3. Department of Mechanical Engineering Code 69 Naval Postgraduate School Monterey, California 93940	1
4. Professor Paul J. Marto Code 69 Mx Department of Mechanical Engineering Naval Postgraduate School Monterey, California 93940	1
5. Kenneth J. Graham, Code 61KG Department of Chemistry and Physics Naval Postgraduate School Monterey, California 93940	1
6. Lieutenant Larry R. Sharp, USN 2029 South Glencove Lane Gretna, Louisiana 70053	1



Thesis
S4354
c.1

Sharp

175367

An apparatus to measure dropwise condensation heat transfer coefficients of steam.

Thesis
S4354
c.1

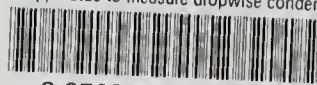
Sharp

175367

An apparatus to measure dropwise condensation heat transfer coefficients of steam.

thesS4354

An apparatus to measure dropwise condens



3 2768 001 94375 6

DUDLEY KNOX LIBRARY